Robustness of Steel Braced Frame to Resist Disproportionate Collapse Caused by Corner Column Removal

Xi Lan[1], Zhi Li[2], Feng Fu[3], Kai Qian[2*]

[1]College of Civil Engineering and Architecture, Guangxi University, Nanning, China, 530004.

[2]Guangxi Key Laboratory of New Energy and Building Energy Saving at Guilin University of Technology, China, 541004.

[3]Department of Engineering, School of Science and Technology at City, University of London, EC1V 0HB U.K.

Abstract:

Steel braces have been widely used as a major lateral stability system to resist the lateral load. However, the influences of steel braces on enhancing the load resistance in moment-resisting steel frames under column removal have not been studied adequately due to the lack of experimental data, especially under worst case scenarios, corner column removal. Thus, five two-floor steel moment-resisting subframes with or without braces were tested by applying a pushdown force. The purpose of this study is to quantify the effects of steel braces on the robustness of steel moment-resisting frames against disproportionate collapse. The test results indicated that steel braces could enhance the ultimate load bearing capacity up by 102.3 %. Compared to V configuration, X configuration is more efficient in increasing the load resistance since a proportion of the vertical load may be transferred to the side column through diagonal braces straightly. The de-composition of the load bearing capacity indicated that compressive braces only affect the initial stiffness and most of the load resistance is attributed to tensile braces for both X and V configurations. De-composition of the load bearing capacity indicated that the load bearing capacity from the first floor is normally greater than that from the second floor due to greater Vierendeel action mobilized.

Author Keywords: Disproportionate collapse; Corner column; Steel frame; Braces; Test

* Corresponding author. Professor, E-mail address: qiankai@glut.edu.cn

1. Introduction

Disproportionate collapse is an event, when the failure of the loss of one or a couple of members, results in the collapse of building disproportionate to the initial local failure. In recent years, the collapses of steel frames occurred frequently, including the landmark building twin towers, in New York in 2001, the steel frame at Xinjia Hotel building in Quanzhou, China in 2020, etc., which have received considerable attention from the public due to catastrophic consequences.

Potential hazards with abnormal load (i.e. vehicular impact, fire, gas explosion, and terrorist attack, etc.) may trigger disproportionate collapse [1-3]. Due to limited alternate load paths of the remaining structure, the removal of columns at corners is more vulnerable than other column missing scenarios. Kim and Kim [4] numerically evaluated the probability of disproportionate collapse of steel moment-resisting frames subjected to various column removal scenarios. They found that the vulnerability of disproportionate collapse was greatest when a corner. column was removed suddenly. Gerasidimis [5] investigated the disproportionate collapse vulnerability of steel frames for the case of a corner column loss and developed an analytical method to capture the collapse mechanism of a steel frame under corner column-removal scenarios. Based on numerical analysis, Fu and Tan [6] studied the disproportionate collapse mechanism of composite floor systems after a corner column was removed. Compared with the results obtained in the case of internal column removal, catenary action and tensile membrane action in beams failed to develop. These studies provided insight into the disproportionate collapse of steel frames after a corner column was removed behavior associated with the removal of corner columns from steel frames. However, other studies [7-12] found that the bending moments of the beam end near the corner joints reversed after the corner column was removed, leading to a significantly bending moment (the bottom subject to tension) developed there. Based on tests on singlefloor beam-column sub-assemblages, most existing studies [13-16] captured the performance of multi-floor steel frames under the scenario of a corner column removal by simplifying them as cantilever beams, which unrealistically ignored the interaction of structural members in different floors (Vierendeel action).

However, structures are not normally designed for the catastrophic consequences provoked by abnormal events. On the other hand, it is not economical to rehabilitate the structures just for the purpose of increasing disproportionate collapse resistance. Thus, design engineers should be aware of the potential vertical load resistance, which had been ignored in conventional design, such as the additional load resistance from masonry infilled walls and steel braces. Xavier et al. [17] tested a steel substructure incorporating infilled walls, which indicated that infilled walls affect the behavior of steel frames significantly. Moreover, Shan et al. [18] investigated the effect of infilled walls on the load resistance of the steel moment frames. They indicated that masonry infill walls could enhance the load bearing capacity and initial stiffness significantly. However, they will change the failure patterns. Seismic investigations had confirmed that the moment resisting frames with braces was an efficient seismic resisting system with sufficient lateral load resistance and stiffness [19, 20]. However, the ability of steel braces to improve the performance of steel frames to resist disproportionate collapse is still unclear. Khandelwal et al. [21] revealed that steel braced frames which were designed to meet seismic requirements could survive even if a column was removed suddenly, since the steel braces are effective in providing additional load resistance. It was found that horizontal braces could be employed to retrofit the steel moment-resisting frame [22]. It was indicated that an additional alternate load path was formed by horizontal braces, and thus, partial loads were directly transferred to the side columns.

However, experimental investigations of steel bracing systems after the removal of a corner column were rare. Moreover, the connections types in previous numerical studies are either pinned or fully restrained [23-25], the behavior of steel braced frames using partially restrained connections is still unclear. In this experimental program, five two-floor and two-bay steel moment-resisting frames were designed and tested after the removal of a corner column removal. The influence of different steel bracing configurations and connection types were quantified experimentally and analytically.

2. Experimental program

2.1. Test specimens

As listed in Table 1, five test specimens including three braced frames (WX, WV, and EX) and two bare frames without any braces (WB and EB), were designed in this experimental program. As the main investigated parameters were the connection types and bracing configuration, the specimens were labeled as follows: the alphabets "W" and "E" represent welded and end-plate connection, respectively. Then, the alphabet of "B", "X", and "V" stand for bare frames, braced frames with X-shaped bracing, braced frames with V-shaped bracings, respectively. Referring to Fig. 1, the prototype frame is designed according to ANSI/AISC 360-05 [20]. The prototype frames had 6×6 bays with a transverse and longitudinal span of 6.0 m and 8.4 m, respectively. The floor height is 3.0 m. The dead load and live load were 5.1 kN/m^2 and 3.0 kN/m^2, respectively. For braced frames, the prototype frame is seismic designed. Site class D was assumed and the critical acceleration parameters S_{DS} and S_{D1} are 0.20 and 0.14, respectively. For bare frames with non-seismic design, identical frames as the braced frames except no braces were installed for comparison. As illustrated in Fig. 1, a two-floor subframe was derived from the prototype frame as a specimen for testing. Considering the limitation of lab and facility, only half-scale sub-frames were tested.

In contrast to the corner column without additional horizontal restraints, overhanging beam (length of 655 mm) was fabricated beyond the side column to consider the horizontal constraints from the interior bays, which will connect with an A-frame by horizontal chain-poles (refer to Fig. 2a). The cross-section of beams and columns is HN 200×100×5.5×8 and HW 150×150×7×10, respectively. Fig. 3 presented the fabrication details of the specimens. For welded connection, complete joint penetration welds were used to connect the beams and columns. For end-plate connection, the beam was welded to an end plate with thickness of 10 mm. Eight M18 Grade 8.8 frictional bolts are employed for bolt connection with a pre-loading force of 345 N·m. The braces and the connections were designed based on ANSI/AISC 341-05 [19]. The braces and beams are connected by the gusset plates welded to the beam flanges. The uniform force method was employed to determine the force acting on welds [26]. To avoid the gusset plate premature yield and fracture occurred in the gusset plate before braces failure, the gusset plate is designed relatively stronger [19, 21]. Taking WX and EX as an example, the braces were made by steel angles with a dimension of 36 ×36 × 4 mm as shown in Fig. 2a. WX and EX have X shaped braces and the size of gusset plate is 330×125×12 mm. In addition, WV has V shaped braces. The gusset plates installed in the second floor have a size of 160×155×12 mm while the gusset plate installed in the first floor has a size of 510×155×12 mm.

2.2. Material properties

All structural members were fabricated by Grade Q235 steel. As displayed in Table 2, the critical material properties of each component are measured via coupon tests in accordance with the relevant specification [27]. The average value of three coupons was calculated for each set of results in this table. The properties of M18bolts were provided by supplier.

2.3. Test setup

As illustrated in Fig. 4a, the ground corner column was not assembled to represent the initial damage. Beneath each side column, a pin support was applied. The vertical load was imposed at the top of corner column through a whisky jack. Displacement-controlled loading method was adopted. At the beginning of the test, a loading rate of 5 mm/min was set until reaching the vertical displacement of 100 mm. In the subsequent loading process, the loading rate of 10 mm/min was adopted. The applied concentrated load was monitored by a load cell, which was placed beneath the whisky jack. To prevent undesirable out-of-plane failure, a steel assemblage was specially arranged.

To represent the axial loads from upper floors, a whisky jack was applied on the side column to guarantee an axial compressive ratio of 0.3. The overhanging girder, if any, was connected to the reaction frame through a horizontal chain-pole. Tensile/compressive load cell was mounted in the horizontal chain-pole, so that the horizontal reaction force could be monitored. To measure the vertical load redistribution to the side column, each pin support was installed a load pin. Above the corner column, a hinge was set to allow the conceivable rotation of the corner column during the test. Moreover, two transverse beams with rollers were mounted at both sides of the corner column to prevent out-of-plane movement during the test. In addition, as shown in Fig. 4a, three LVDTs were mounted along the beam of first floor in the corner bay. It should be mentioned that the deflection of beam between side columns was negligible during the test of Specimen WB, thus they were not monitored in the following tests. As given in Fig. 2, to determine the variations of the axial forces and bending moments in the beams, a series of strain gauges were attached to the critical sections.

3. Test results

In order to assess the robustness of steel bending-moment frames with steel braces, five two-floor steel sub-frames with or without bracings were experimentally tested after a corner column loss. The key results are tabulated in Table 3 and presented below.

3.1 Global behavior

WB: The load-displacement curves at the corner column of WB, WX, and WV are displayed in Fig. 5. The specimens initially exhibited elastically as the load resistance increased linearly. The yield load was measured to 64.7 kN at the corner column deflection (CCD) increased to 80 mm. Thus, it has initial stiffness of 0.8 kN/mm. The initial stiffness was defined as the ratio of yield load to yield displacement herein. The load resistance started to decrease after the occurrence of local buckling at beam flanges in the first floor, which was attributed to the effects of flexural bending. At an CCD of 233 mm, the ultimate load bearing capacity, which was defined as the peak load resistance, of 78.2 kN was reached. On further increasing the displacement, similar local buckling also occurred at beam flanges in the second floor at CCD of 400 mm. Fig. 6 shows the failure pattern of the specimen. Although no fracture occurred during the test, the local buckling was severe at the beam ends, which resulted in the beam of the first floor failing in torsion in absence of catenary action.

WX: As the second floor has X braces, the failure pattern of WX was changed. In the start of testing, the compressive braces started to buckle, which indirectly showed that the compressive braces may have little contribution to the load enhancement. This can be confirmed by the strain gauge results later. As displayed in Fig. 5, it has a yield load of 116.5 kN at an CCD of 62 mm. Moreover, it has initial stiffness of 1.9 kN/mm, about 232.3% of that of WB. Similar to WB, local buckling of the bottom beam flange occurred near the side column in the ground floor at this stage. It has an ultimate load bearing capacity of 125.4kN. The tensile brace fractured at an CCD of 288 mm, which leads to the load resistance dramatically dropping from 74.9 kN to 24.3 kN. Fig. 7 gives the failure pattern of the specimen. Tensile braces were fractured and compressive braces were severely buckled. No yielding was observed in the gusset plates. Similar to WB, torsional damage occurred in the beam in the first floor. However, premature weld fractures occurred in Joints S1, S2 and C2 of WX, which were not observed in WB. This was due to the additional shear forces from the steel braces and the torsion-induced shear forces in the beams.

WV: For WV, it has a yield load of 93.5 kN and initial stiffness of 1.9 kN/mm. Similar to WX, the compressive braces began to out-of-plane buckling at the very beginning of the load. Different from WX, the tensile brace fractured at a relatively early stage (corresponding to CCD of 63 mm) and followed by the drop in load resistance dramatically. Moreover, it has an ultimate load bearing capacity of 100.9 kN, which is 129.0% and 80.5% of that of WB and WX, respectively. When the fracture occurred at the beam ends, the load resistance dropped significantly. After reaching the CCD of 191 mm, the load bearing capacity of WV became even lower than that of WB. Fig. 8 displays the failure pattern of WV. Similar to WX, the compressive braces suffered severe buckling and the tensile braces were fractured. However, different from WX, there is no torsional damage occurring in the beams with gusset plate welded to the beam flange were enough to prevent torsional buckling.

EB: Fig. 9 compares the load-displacement curves of EB and EX. EB achieved a yield load of 42.7 kN and initial stiffness of 0.7 kN/mm. When the CCD reached 135 mm, the welds nearby the side column in the second floor fractured. Subsequently, the load bearing capacity could increase until further weld fracture occurred at the end-plate. It has an ultimate load bearing capacity of 55.5 kN. Similar fractures occurred at the beam ends near the corner column at CCD of 406 mm and 487 mm, respectively. Fig. 10 gives the failure pattern of the specimen. The failure of EB was controlled by weld failure at the end-plate.

EX: It has a yield load of 86.4 kN and initial stiffness of 1.9 kN/mm. The weld fracture was initially developed nearby the corner column. With the displacement kept increasing to 128mm, EX reached its ultimate load bearing capacity of 105.8 kN. When CCD increased to 159 mm and 336 mm, the welds fracture was formed at the beam ends in sequence. The tensile braces fractured at an CCD of 602 mm, which was 109.0% later than WX. Fig. 11 gives the failure pattern of EX. Similarly, the compressive brace suffered severe out-of-plane buckling while the tensile brace fractured. Moreover, local buckling occurred at point A.

3.2 Deformation measurements

The deformation shape of beams at different stages is displayed in Fig. 12. Following DoD [28], the chord rotation was defined as the ratio of CCD to beam span. From the figure, the chord rotation would significantly underestimate the rotation of the beam end nearby the corner column. On the other hand, the chord rotation could assess the rotation of the beam end nearby the side column accurately, especially for WX and WV. The external steel brace would not significantly change the deflection shape of the beams. Similar observation was achieved in EB and EX.

3.3 Internal force evaluation

To deeply understand the contribution of load resistance from braces, the contribution of braces and frames should be determined individually. Before that, the reliability of calculation formula to determine the internal force of each component based on strain gauge results must be verified. From Fig. 2a, Sections B1-4 installed a series of strain gauges, which could help to determine the internal force. Similar to the calculation method proposed in the previous paper [29, 30], the load-displacement curve based on strain gauge data was determined and compared with the one from load cell results (refer to Fig. 13). As shown in Fig. 13, good agreements are achieved between the one measured by the load cell and analytical results from strain gauge data. For WX and EX, the minor discrepancy of initial stiffness may be caused by unavoidable gaps in the test setup, which did not reflect in the LVDT placed above the corner column. Generally, the analytical results based on strain gauges can well capture the character of the curve until failure.

Fig. 14 presents the load bearing capacity of the braces and frame. Relying on the analytical results of internal force, it was revealed that the load bearing capacity from the bare frame was purely provided by flexural action, the contribution of catenary action could be ignored due to the limited tensile forces in the beams. For WX, at the ultimate load resistance stage, the contribution of steel braces was about 35.3%. With the increasing vertical displacement, the load resistance of the steel braces began to decrease due to the yield of beam section releasing the constraints for the tensile braces gradually. For WV, at the stage of ultimate load bearing capacity, the contribution of steel bracing was only 27.7% as the tensile braces fractured. Different from the braced frames with welded connection, for EX, initially, the steel braces contributed greater load resistance than the frame. At the stage of ultimate load resistance, the contribution of steel braces was 45.7%, which was comparable to that of the frame. Moreover, after that, the load resistance from braces is always comparable to that from frames until the test final.

4. Discussion of experimental results

4.1 Contribution of load resistance

The de-composition of the frame contribution from each floor is given in Fig. 15. As shown in the figures, the load bearing capacity from the first and second floor has similar trends until failure occurred in the connections, while the first floor has slightly greater load resistance than that of second floor. This was due to the greater rotational constraints and Vierendeel action, for which further explanation would be in section 4.2. However, WX had a greater maximum load resistance from the second floor as the connection in the first floor fractured earlier.

Fig. 16 displays the de-composition of load bearing capacity contribution from tensile brace and compressive brace. For WB, WX, and WV, the maximum load resistance from steel braces was 46.4, 29.7, and 49.8 kN, respectively. Different from WX and EX, which reached their maximum load resistance until the tensile brace yielded, the maximum load resistance of WV was obtained when the compressive brace buckled. For WV, the compressive brace contributed the maximum load resistance of 14.5 kN, which was 33.7% and 41.2% higher than that of WX and EX, respectively. To better understand the contribution of steel braces, the development of axial force of tensile brace and compressive brace was normalized, as shown in Fig. 17. The tensile brace has an analytical yield load of 85.6 kN. And the compressive brace has buckling loads of 23.0 kN and 57.6 kN for X and V configuration, respectively. As can be seen in the figure, both the tensile and compressive brace in X configuration achieved their yield and buckling loads. However, in V configuration, the tensile brace could not achieve the analytical yield load and the compressive brace could not reach the analytical buckling load as the constraints applied at the braces of V configuration were not translation fixed, which is assumed in analytical analysis.

4.2 Effects of connection types

Unlike braced frames where the maximum deformation would be introduced by the failure of the steel bracing, the maximum deformation of bare frames difficult to identify from the load-displacement curve. The deformation capacities of bare frame were defined as vertical displacement at ultimate load bearing capacity. For WB and EB, the maximum deformation was 233 and 228 mm, respectively. Thus, WB and EB had a similar maximum deformation, which was quite different from the case of missing a middle column [29, 30]. WB was able to sustain large deformation caused by the torsion developed in beams, and avoided the brittle weld fracture. Fig. 18 shows the development of bending moments at the beam ends. From the figure, not only the beam end near the side column, the beam end near the corner column also experienced large positive bending moments, which was different from the behavior of unsupported cantilevers. This indicated that Vierendeel action played an important role in the load resisting mechanism after corner column removal. Moreover, DoD [28] defined the acceptable plastic rotation angles for different type of steel connections. Taking Section 1B1 as an example, the parameters ‘a’ and ‘b’ were defined as shown in Fig. 18. Table 4 compared the measured parameters with the requirements in specification, which showed that the recommended ductility acceptance criteria were conservative for both fully and partially restrained moment connections in current specimens.

Although this experimental test was focused on the static performance of welded and endplate connections, disproportionate collapse following sudden column removal exhibits a typical dynamic response. Based on the available static load-displacement curve, a dynamic capacity evaluation was applied using an energy-based method proposed by Izzuddin et al. [31]. This approach has been applied and verified in previous studies related to disproportionate collapse [32-34]. As described in Eq. (1), the equivalence between external work (dynamic response) and internal energy (static response) was used to obtain the dynamic response shown in Fig. 19.

$$P_d\left(u_d\right) = \frac{1}{u_d}\int_0^{u_d} P_{NS}(u)du \tag{1}$$

As labeled in Fig. 19, the maximum dynamic load capacities of WB, EB, WX, and EX were 65.5, 45.8, 106.7, and 93.2 kN, respectively. Prior to this point being reached, it was unlikely for the specimens to undergo disproportionate collapse even if a sudden column failure occurred. The maximum dynamic deformations of WB, WX and WV were 380, 380, 200 and 320 mm, which were 163%, 194%, 167% and 250% of that of maximum static deformations, respectively. This implied that the deformation capacity of the frames under sudden column removal were greater than those under quasi-static loading for the same applied load.

4.3 Effects of braces types

As seen from Fig. 5, the yield load of WB, WX, and WV were 64.7, 116.5 and 93.5 kN, respectively. Therefore, the X and V braces enhanced the yield load of WB by 80.1% and 44.5%, respectively as the X bracing configuration in WB can directly transfer a portion of the load to the side column. Regarding the ultimate load bearing capacity, WB, WX and WV were 78.2, 125.4 and 100.9 kN, respectively. Therefore, the X and V bracing configuration enhanced the ultimate load bearing capacity of WB by 60.4% and 29.0%, respectively. This could be attributed into the tensile braces in V configuration fractured much earlier, even earlier than the yielding of the beams. Moreover, the maximum deformation of WB, WX and WV were 233, 288 and 63mm, respectively. Thus, the steel bracing with X configuration increased the maximum deformation of WB by 23.6%, while the steel bracing with V configuration decreased the maximum deformation of WB by 73.0%. The maximum deformation of WX was 457.1% of that of WV. Regarding to failure patterns, as shown in Fig.12, torsional damage occurred at interfaces between the beam and corner column joint of WB and WX [35, 36]. However, due to the gusset plate of V bracing configuration, the critical beam section shifted close to the beam midspan, which prevented the torsional damage of WV [37].

5. Conclusions

A series of five two-bay and two-floor steel sub-frames were tested subjected to a corner column missing scenario to investigate the robustness of steel braced frames to resist disproportionate collapse. Following conclusions are obtained:

1. Steel braces could increase the initial stiffness and load resistance of steel frames whatever X configuration or V configuration was adopted. However, torsion may control the failure of bare frame, while the braces also amplified the shear force demand at the beam ends. Therefore, it is necessary to consider the torsional shear forces of adjacent structures where corner column is removed in the alternate load path method. The connection design can be controlled by the shear forces generated by torsion, especially for braced frame.
2. Experimental results indicated that the tensile braces in steel frames with end-plate connections did not fracture until the vertical deformation reached 20% of the beam span. X configuration performed better than V configuration regarding ultimate load bearing capacity and initial stiffness, as X configurations could transfer partial of the load to the side column directly while V configuration are only subjected to axial forces within the elastic range. Whatever X or V configurations, the compressive braces only affect the initial stiffness as they were severely buckled from the very early beginning of the test.
3. Different from the scenario of loss of an interior column, the bare frame with weld connection achieved a similar maximum deformation than that of steel frame with end-plate connections when the scenario of corner column missing was concerned. Moreover, the value of plastic hinge properties was too conservative for the bare frame with weld connection and end-plate connection under corner column removal.
4. Analytical analysis found that the load resistance of the frame in the ground floor is generally larger than that in the second floor because the structural components in the second floor could provide horizontal constraints to the joints in the ground floor, in other words, greater Vierendeel action was mobilized in the frames in the ground floor.

Acknowledgements

The authors gratefully acknowledge the financial support provided by the National Natural Science Foundation of China (Nos. U22A20244 and 52022024) and Natural Science Foundation of Guangxi (No.2021GXNSFFA196001). Any opinions, findings and conclusions expressed in this paper do not necessary reflect the view of National Natural Science Foundation of China and Natural Science Foundation of Guangxi.

References

[1] B.R. Ellingwood, R. Smilowitz, D.O. Dusenberry, D. Duthinh, H. Lew, N.J. Carino, Best practices for reducing the potential for progressive collapse in buildings, National Institute of Standards and Technology, Gaithersburg, Maryland, U.S.A. (2007).

[2] D.C. Feng, M.X. Zhang, E. Brunesi, F. Parisi, Y. Jun, Z. Zhen, Investigation of 3D effects on dynamic progressive collapse resistance of RC structures considering slabs and infill walls, J. Build. Eng. 54(15) (2022) 104421. https://doi.org/10.1016/j.jobe.2022.104421.

[3] I.M.H. Alshaikh, B.H.A. Bakar, E.A.H. Alwesabi, A.A. Abadel, H. Alghamdi, A. Altheeb, R. Tuladhar, Progressive collapse behavior of steel fiber-reinforced rubberized concrete frames, J. Build. Eng. (2022) 104920. https://doi.org/10.1016/j.jobe.2022.104920.

[4] J. Kim, T. Kim, Assessment of progressive collapse-resisting capacity of steel moment frames, J. Constr. Steel Res. 65(1) (2009) 169-179. https://doi.org/10.1016/j.jcsr.2008.03.020.

[5] S. Gerasimidis, Analytical assessment of steel frames progressive collapse vulnerability to corner column loss, J. Constr. Steel Res. 95 (2014) 1-9. https://doi.org/10.1016/j.jcsr.2013.11.012.

[6] Q. N. Fu, Tan, K. H, Numerical study on steel-concrete composite floor systems under corner column removal scenario, Structures. 21, (2019) 33-44. https://doi.org/10.1016/j.istruc.2019.06.003.

[7] M. Sasani, S. Sagiroglu, Progressive collapse resistance of Hotel San Diego, J. Struct. Eng. 134(3) (2008) 478-488. https://doi.org/10.1061/(ASCE)0733-9445(2008)134:3(478).

[8] I. Azim, J. Yang, S. Bhatta, F.L. Wang, Q.F. Liu, Factors influencing the progressive collapse resistance of RC frame structures, J. Build. Eng. 27 (2022) 100986. https://doi.org/10.1016/j.jobe.2019.100986

[9] K. Qian, B. Li, Z. Zhang, Influence of multicolumn removal on the behavior of RC floors, J. Struct. Eng. 142 (2016) 04016006. https://doi.org/10.1061/(ASCE)ST.1943-541X.0001461.

[10] A.T. Pham, N.S. Lim, K.H. Tan, Investigations of tensile membrane action in beam-slab systems under progressive collapse subject to different loading configurations and boundary conditions, Eng. Struct. 150 (2017) 520-536. https://doi.org/10.1016/j.engstruct.2017.07.060.

[11] J. Z. Zhang, B. Jiang, R. Feng, R. Chen, Robustness of steel moment frames in multi-column-removal scenarios, J. Constr. Steel Res. 175, (2020) 106325. https://doi.org/10.1016/j.jcsr.2020.106325.

[12] K. Qian, X. Lan, Z. Li, F. Fu, Behavior of steel moment frames using top-and-seat angle connections under various column removal scenarios, J. Struct. Eng. 147 (10) (2021) 04021144. https://doi.org/10.1061/(ASCE)ST.1943-541X.0003089.

[13] W. Wang, J.J. Wang, X. Sun, Y.H. Bao, Slab effect of composite subassemblies under a column removal scenario, J. Constr. Steel Res. 129(2) (2017) 141-155. https://doi.org/10.1016/j.jcsr.2016.11.008.

[14] P.M. Stylianidis, D.A. Nethercot, B.A. Izzuddin, A.Y. Elghazouli, Study of the mechanics of progressive collapse with simplified beam models, Eng. Struct. 117 (2016) 287-304. https://doi.org/10.1016/j.engstruct.2016.02.056.

[15] J. Hou, L. Song, H.H. Liu, Testing and analysis on progressive collapse-resistance behavior of RC frame substructures under a side column removal scenario, J. Perform. Constr. Facil. 30(5) (2016) 04016022. https://doi.org/10.1061/(ASCE)CF.1943-5509.0000873.

[16] O. A. Mohamed, Assessment of progressive collapse potential in corner floor panels of reinforced concrete buildings, Eng. Struct. 31(3) (2009) 749-757. https://doi.org/10.1016/j.engstruct.2008.11.020.

[17] F.B. Xavier, L. Macorini, B.A. Izzuddin, C. Chisari, N. Gattesco, S. Noe, C. Amadio, Pushdown tests on masonry infilled frames for assessment of building robustness, J. Struct. Eng. 143(9) (2017) 04017088. https://doi.org/10.1061/(ASCE)ST.1943-541X.0001777.

[18] S.D. Shan, S. Li, S.H. Wang, Effect of infill walls on mechanisms of steel frames against progressive collapse, J. Constr. Steel Res. 162 (2019) 105720. https://doi.org/10.1016/j.jcsr.2019.105720.

[19] American Institute of Steel Construction, Seismic Provisions for Structural Steel Buildings, ANSI/AISC 341-05, Chicago, Illinois, U.S.A. (2005).

[20] American Institute of Steel Construction, Specifications for Structural Steel Buildings, ANSI/AISC 360-05, Chicago, Illinois, U.S.A. (2005).

[21] K. Khandelwal, S. El-Tawil, F. Sadek, Progressive collapse analysis of seismically designed steel braced frames, J. Constr. Steel Res. 65(3) (2009) 699-708. https://doi.org/10.1016/j.jcsr.2008.02.007.

[22] J. Chen, W. Peng, R. Ma, Strengthening of horizontal bracing on progressive collapse resistance of multistory steel moment frame, J. Perform. Constr. Facil. 26 (2012) 720-724. https://doi.org/10.1061/(ASCE)CF.1943-5509.0000261.

[23] J. Jiang, G. Q. Li, A, Usmani, Progressive collapse resistance of braced steel frames exposed to fire, Proceedings of the international conference on sustainable development of critical infrastructure (CDRM 8), Shanghai, China, May (2014).

[24] J. Kim, Y. Lee, H. Choi, Progressive collapse resisting capacity of braced frames, Struct. Des. Tall Spec. 20 (2011) 257-270. https://doi.org/10.1002/tal.574.

[25] B. Asgarian, F. H. Rezvani, Progressive collapse analysis of concentrically braced frames through EPCA algorithm, J. Constr. Steel Res. 70 (2012) 127-136. https://doi.org/10.1016/j.jcsr.2011.10.022.

[26] R.M. Richard, Analysis of large bracing connection designs for heavy construction, Proceedings of the 38th AISC National Engineering Conference, Chicago, Illinois, U.S.A, December. (1986).

[27] American Society for Testing and Materials (ASTM), Standard Test Methods and Definitions for Mechanical Testing of Steel Products, ASTM Standard A370-02, Philadelphia, PA (2002).

[28] DoD, Design of Building to Resist Progressive Collapse (UFC 4-023-03), Department of Defense, Washington D.C., U.S.A. (2009)

[29] K. Qian, X. Lan, Z. Li, Y. Li, F. Fu, Progressive collapse resistance of two-storey seismic configured steel sub-frames using welded connections, J. Constr. Steel Res. 170 (2020) 106117. https://doi.org/10.1016/j.jcsr.2020.106117.

[30] K. Qian, X. Lan, Z. Li, F. Fu, Effects of steel braces on robustness of steel frames against progressive collapse, J. Struct. Eng. 147 (11) (2021) 04021180. https://doi.org/10.1061/(ASCE)ST.1943-541X.0003161.

[31] B.A. Izzuddin, A.G. Vlassis, A.Y. Elghazouli, D.A.Nethercot, Progressive collapse of multi-storey buildings due to sudden column loss-Part I: simplified assessment framework, Eng. Struct. 30(5) (2008) 1308-1318. https://doi.org/10.1016/j.engstruct.2007.07.011

[32] Y.H. Weng, K. Qian, F. Fu, Q. Fang, Numerical investigation on load redistribution capacity of flat slab substructures to resist progressive collapse, J. Build. Eng. 29 (2020) 101109. https://doi.org/10.1016/j.jobe.2019.101109

[33] Y.H. Weng, F. Fu, K. Qian, Punching shear resistance of corroded slab-column connections subjected to eccentric load, J. Struc. Eng. 159(1) (2023) 04022219. https://doi.org/10.1061/(ASCE)ST.1943-541X.0003504

[34] K. Qian, B. Li, Effects of masonry infill wall on the performance of RC frames to resist progressive collapse, J. Struct. Eng. 143(9) (2017) 04017118. https://doi.org/10.1061/(ASCE)ST.1943-541X.0001860

[35] A. E. Mcmullen, B. V. Rangan, Pure tension in rectangular sections - a Re-examination, ACI Journal. 75(10) (1978) 511-519. https://doi.org/10.14359/10963.

[36] K. N. Rahal, M. P Collins, Analysis of sections subjected to combined shear and torsion-a Theoretical model, ACI Struct. J. 92(4), (1995) 459-469. https://doi.org/10.14359/995.

[37] A. T. Pham, D. P. Xuan, K. H. Tan, Slab-corner effect on torsional behaviour of perimeter beams under missing column scenario, Mag. Concrete Res. 71(12) (2018) 1-43. https://doi.org/10.1680/jmacr.18.00011.

Table 1. Summary of specimen

Specimen ID	Connection	Bracing configurations
WB	Welded	N/A
WX	Welded	X-shaped braces
WV	Welded	V-shaped braces
EB	End-plate	N/A
EX	End-plate	X-shaped braces

Table 2. Material properties

Items	Plate thickness (mm)	Yield strength (MPa)	Yield strain	Ultimate strength (MPa)	Ultimate strain	Elongation (%)
Beam flange	8	310	0.0019	420	0.024	12
Beam web	5.5	320	0.0021	430	0.0249	13.5
Column flange	10	300	0.0019	410	0.0267	14
Column web	7	295	0.0023	375	0.0242	13
Steel brace	4	310	0.0021	420	0.0256	12.5

Table 3. Test results

Test ID	U_{YL} (mm)	F_{YL} (kN)	K_{YL} (kN/mm)	U_{PL} (mm)	F_{PL} (kN)
WB	80	64.7	0.8	233	78.2
WX	62	116.5	1.9	103	125.4

WV	49	93.5	1.9	63	100.9
EB	60	42.7	0.7	228	55.5
EX	46	86.4	1.9	128	105.8

Note: F_{YL} and F_{PL} represent yield load and ultimate load bearing capacity, respectively; U_{YL} and U_{PL} represent displacements corresponding the yield load and ultimate load bearing capacity, respectively; K_{YL} represents initial stiffness corresponding the yield load.

Table 4. Comparison of the measured and recommended plastic hinge parameters in DoD [28]

Test ID	Section	'a' at the beam end (rad)	'a' in DoD [28] (rad)	'b' at the beam end (rad)	'b' in DoD [28] (rad)
WB	1B1	0.070	0.025	N/A	0.038
	1B5	0.073	0.025	N/A	0.038
	2B1	0.118	0.025	N/A	0.038
	2B5	0.093	0.025	N/A	0.038
EB	1B1	0.050	0.012	0.109	0.018
	1B5	0.063	0.012	0.084	0.018
	2B1	0.094	0.012	0.136	0.018
	2B5	0.026	0.012	0.061	0.018

List of Figures

Fig. 14. De-composition of the load bearing capacity from frame and braces

Fig. 15. De-composition of load bearing capacity from the 1st floor and 2nd floor

Fig. 16. De-composition of the load bearing capacity from tensile brace and compressive brace

Fig. 17. Axial force of braces: (a) tensile brace; (b) compressive brace

Fig. 18. Bending moment development at the beam ends: (a) WB; (b) EB

Fig. 19. Comparison of the static and dynamic load resistance: (a) WB and EB; (b) WX and EX

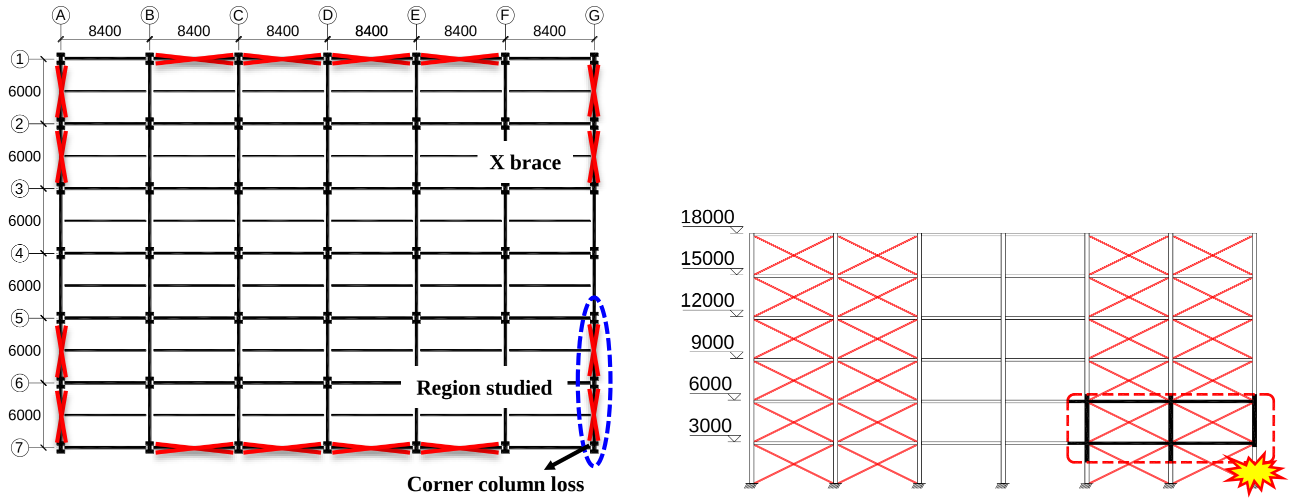

(a) (b)

Fig. 1. Prototype building and extracted frame (unit in mm): (a) front view; (b) side view

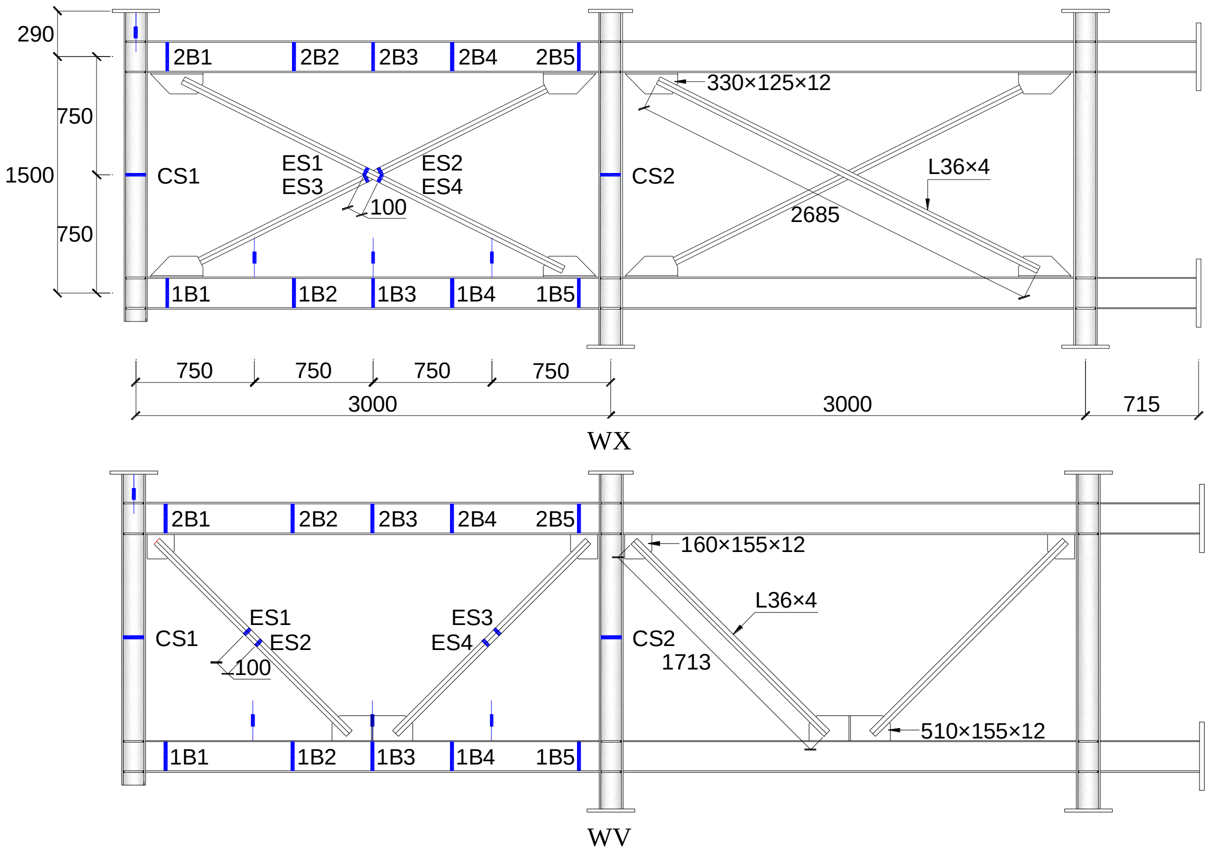

(a)

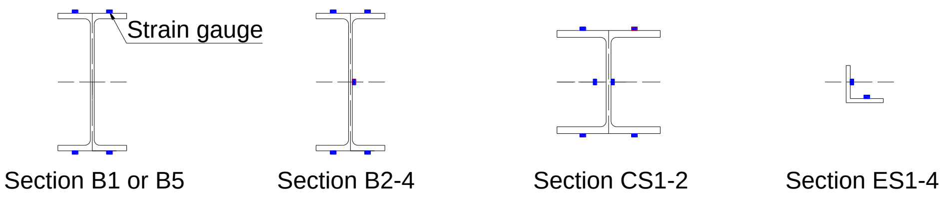

(b)

Fig. 2. Dimensions of the specimen and locations of instrumentations: (a) layout of strain gauge and displacement transducer; (b) position of strain gauges on sections

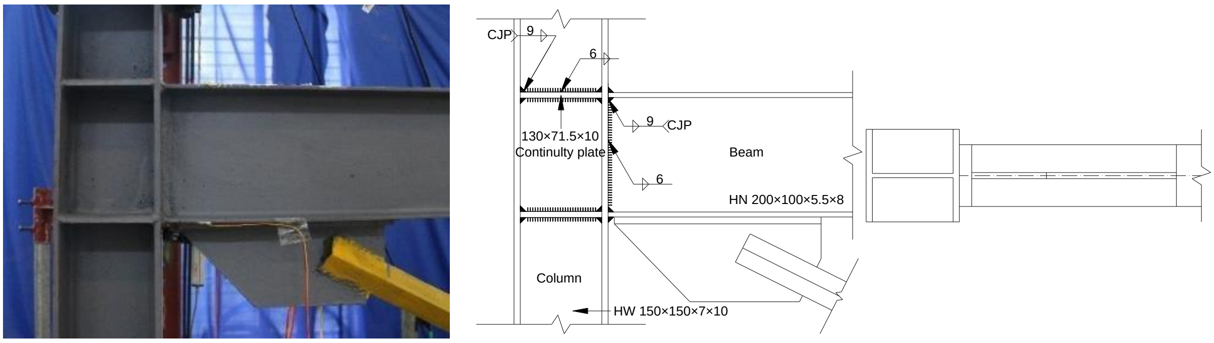

(a)

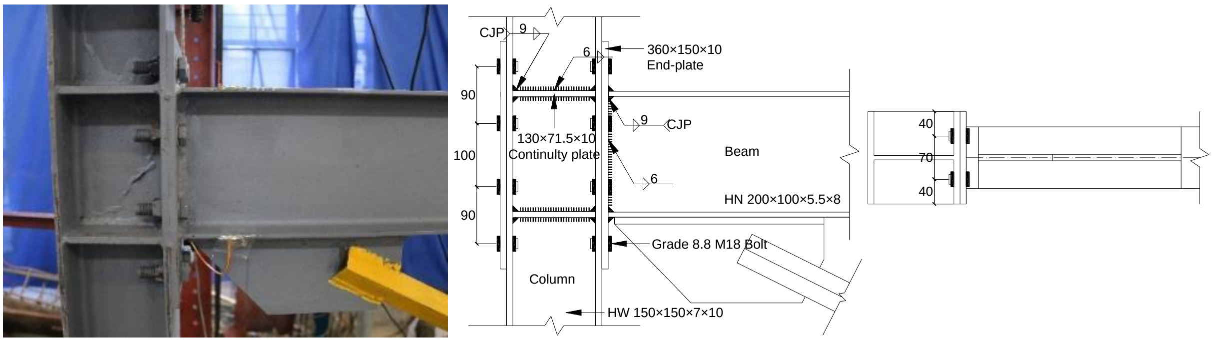

(b)

Fig. 3. Details of the connections: (a) welded connection; (b) end-plate connection

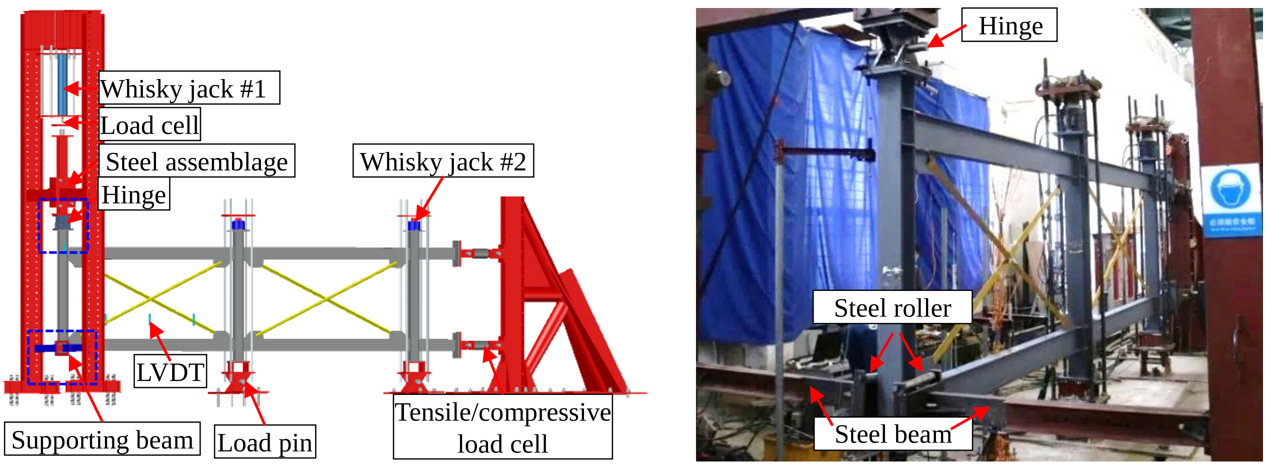

(a) (b)

Fig. 4. Test setups of WX: (a) drawing; (b) photo

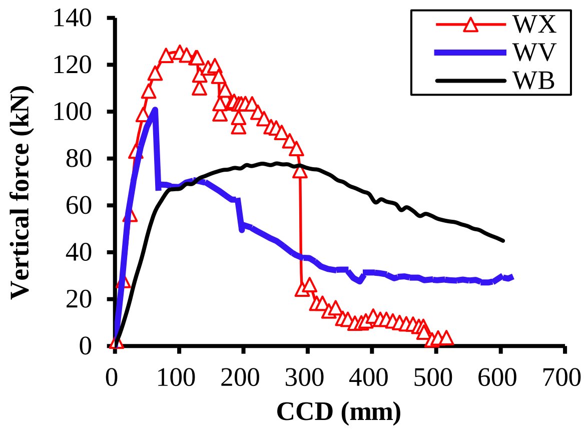

Fig. 5. Load-displacement curves of specimens: WB, WX and WV

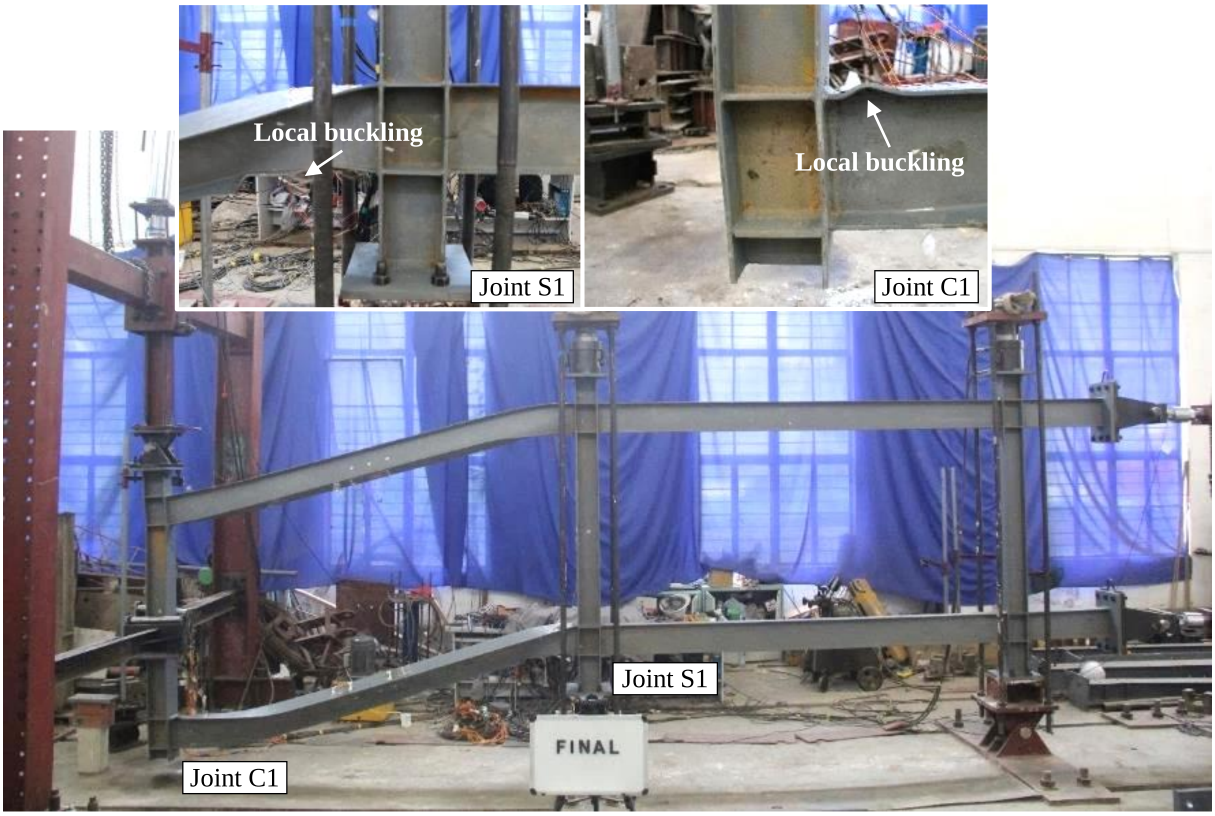

Fig. 6. Failure pattern of Specimen WB

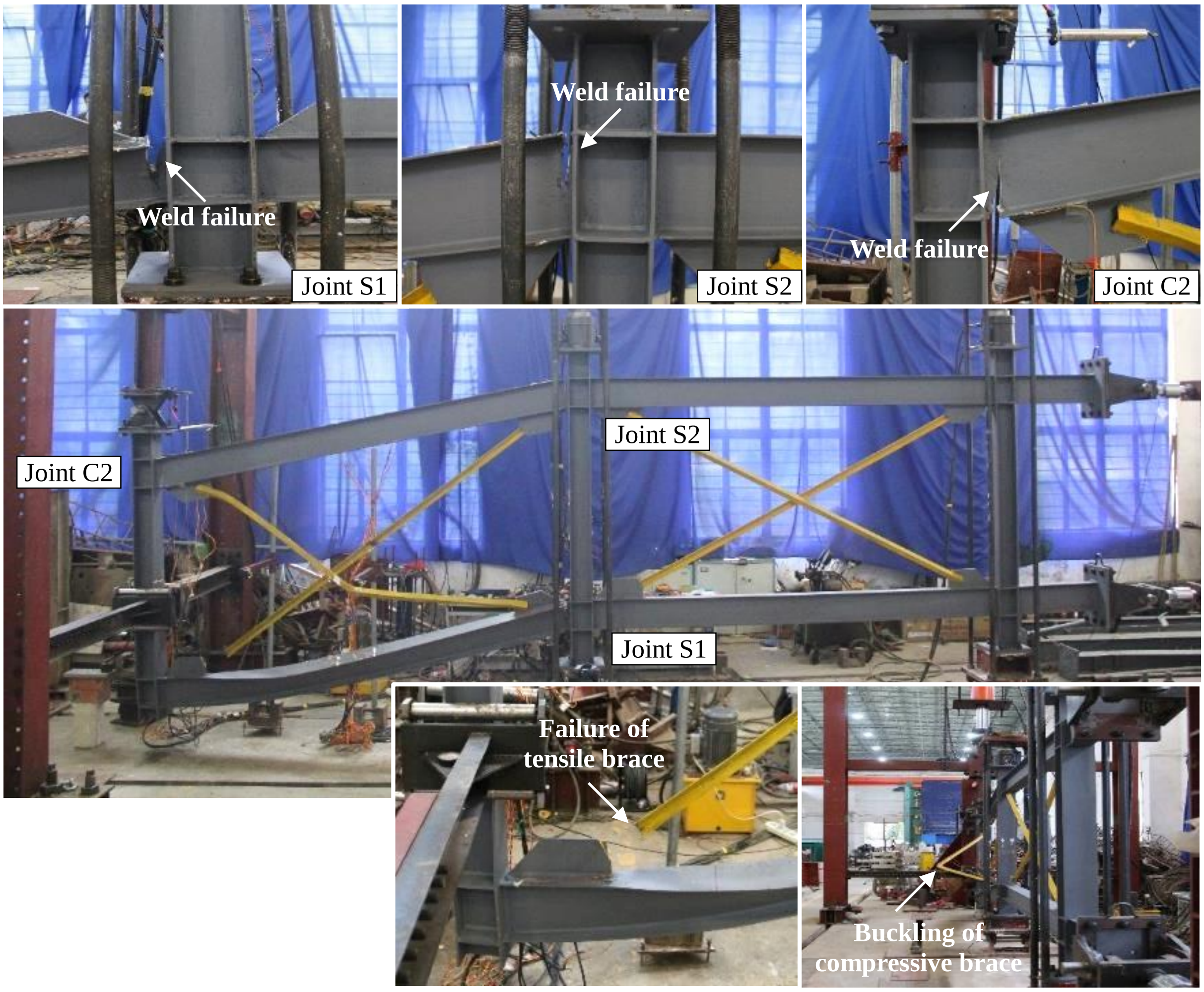

Fig. 7. Failure pattern of Specimen WX

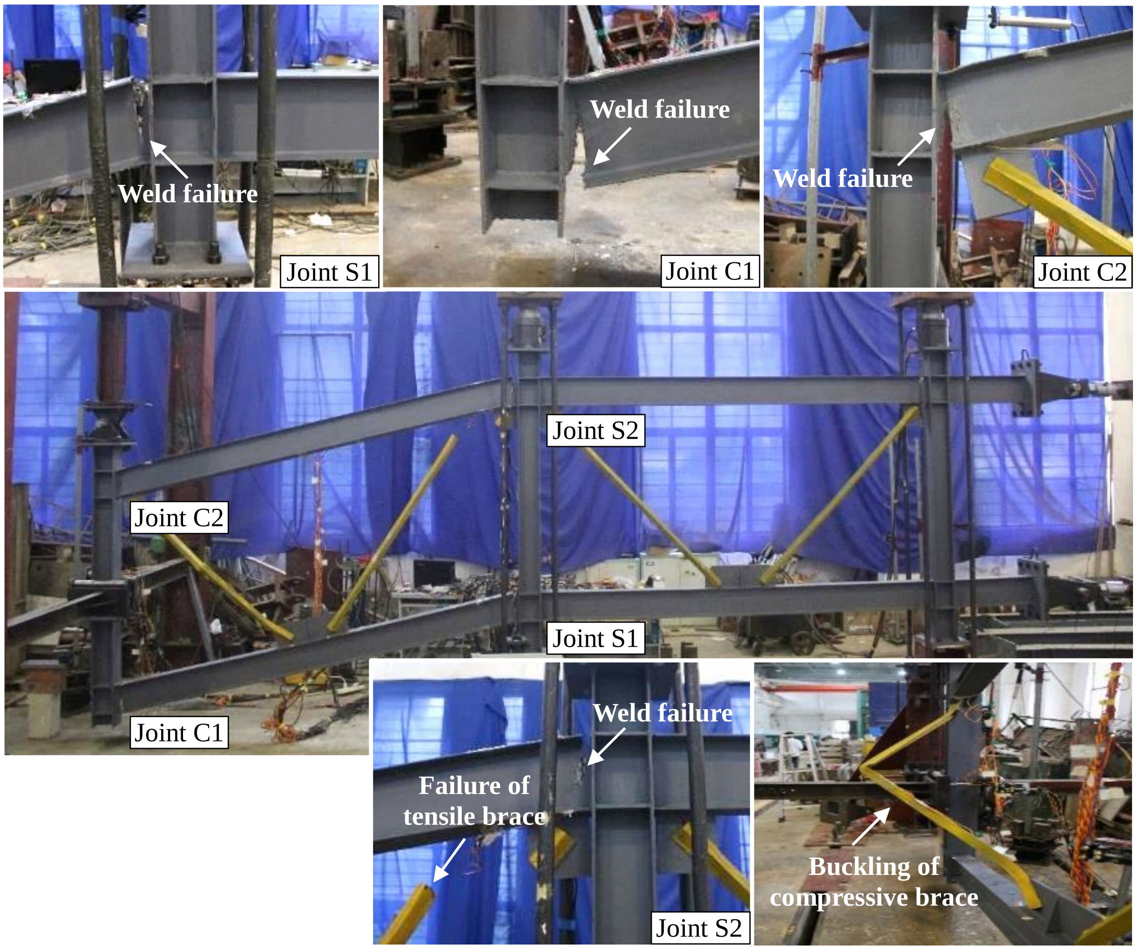

Fig. 8. Failure pattern of Specimen WV

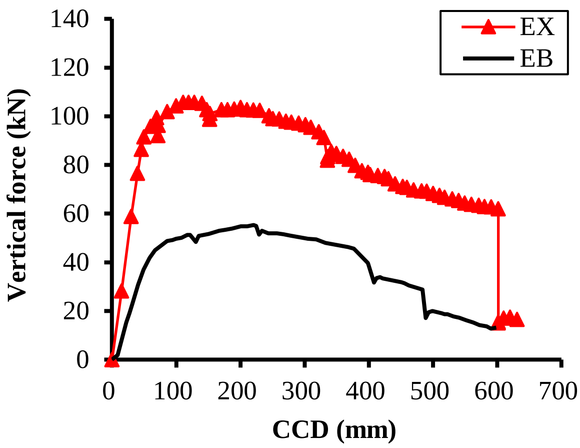

Fig. 9. Load-displacement curves of specimens: EB and EX

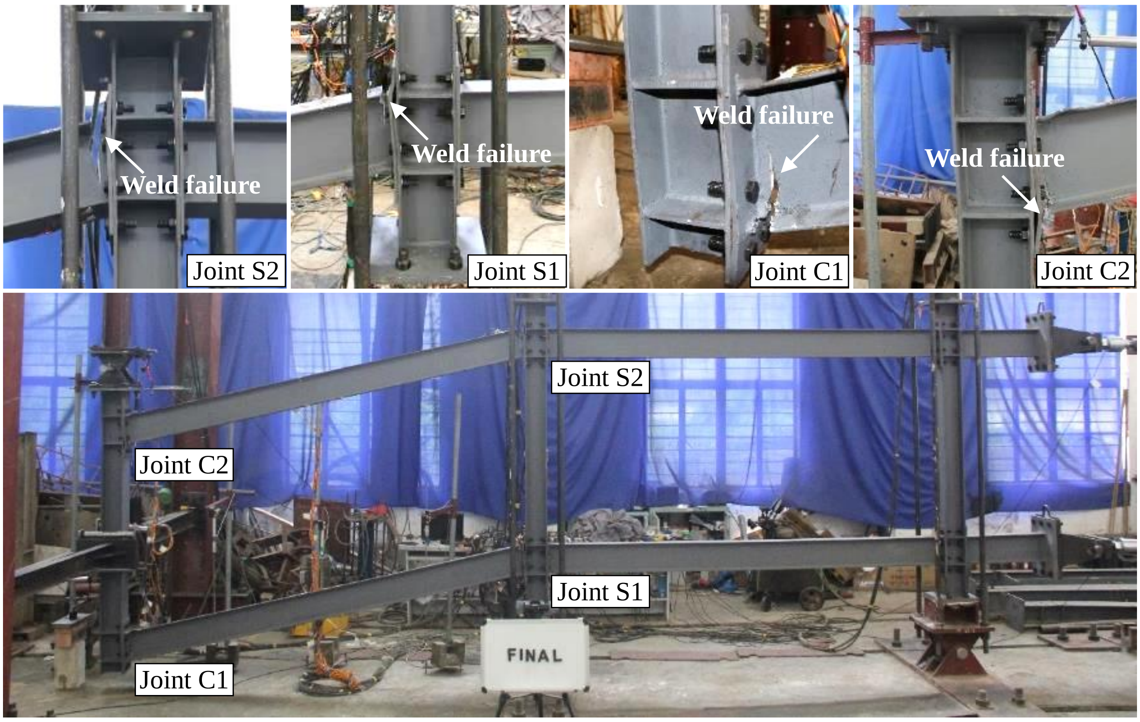

Fig. 10. Failure pattern of Specimen EB

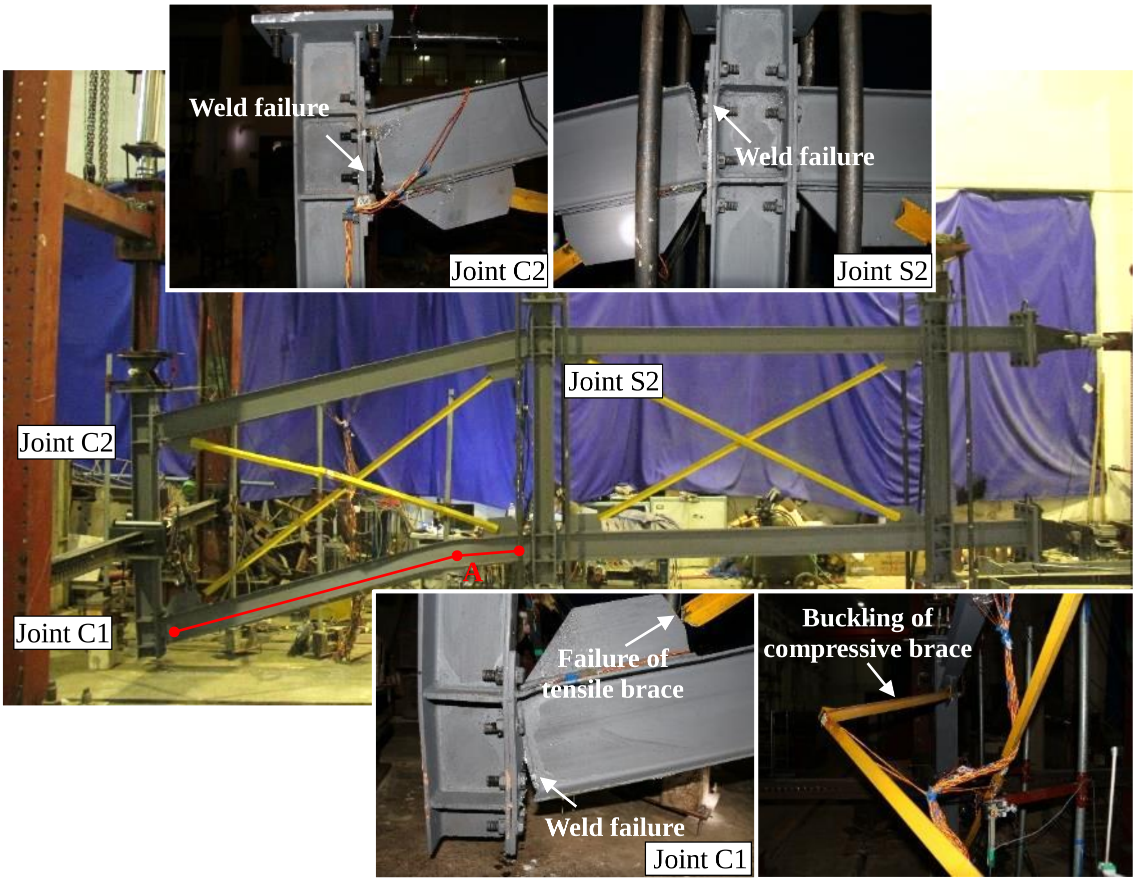

Fig. 11. Failure pattern of Specimen EX

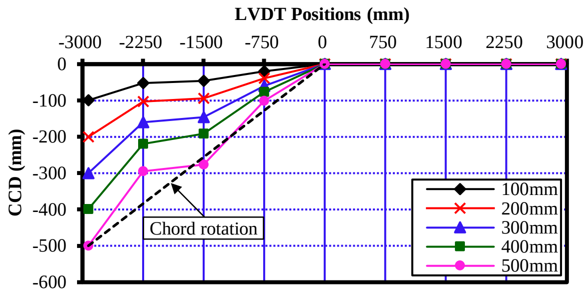

(a)

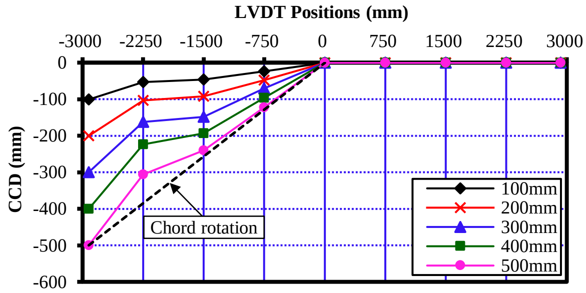

(b)

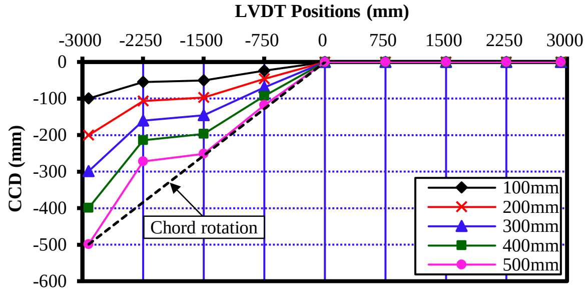

(c)

Fig. 12. Deflection profile of the beams in different stages: (a) WB; (b) WX; (c) WV

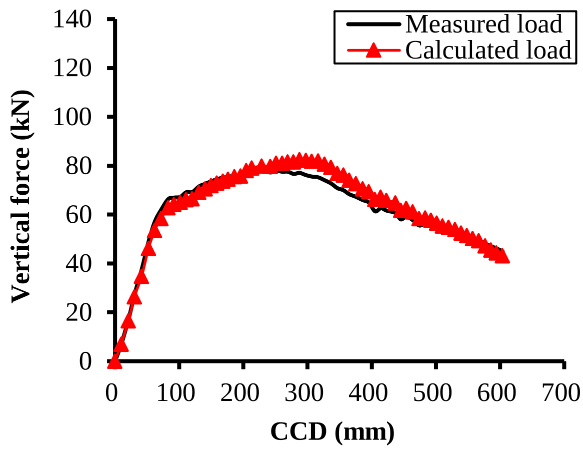

(a)

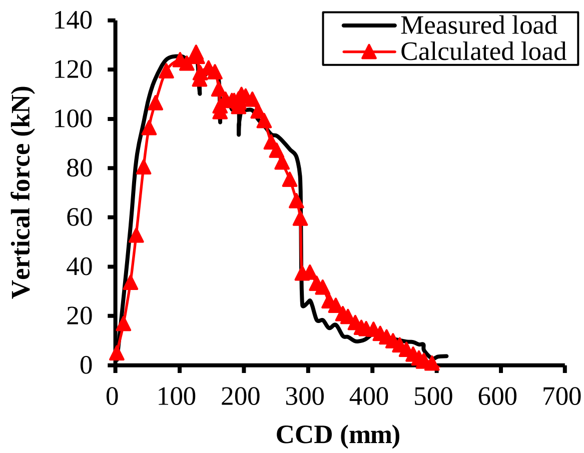

(b)

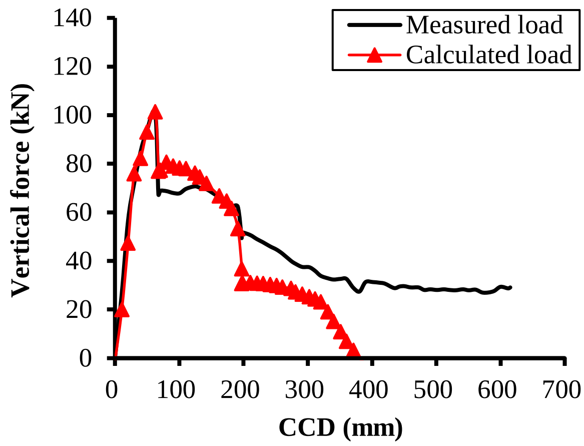

(c)

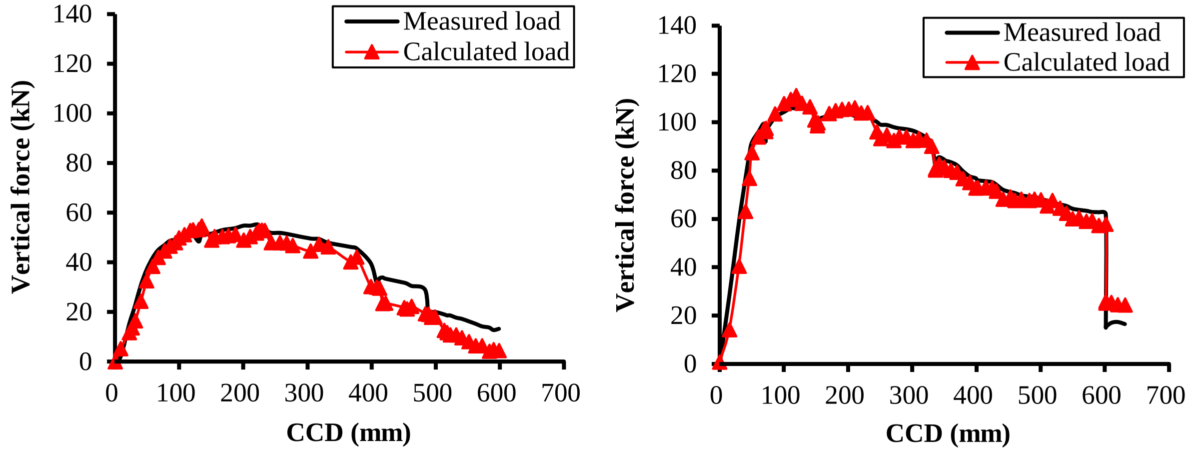

(d) (e)

Fig. 13. Load-displacement curves from strain gauge and load cells: (a) WB; (b) WX; (c) WV; (d) EB; (e) EX

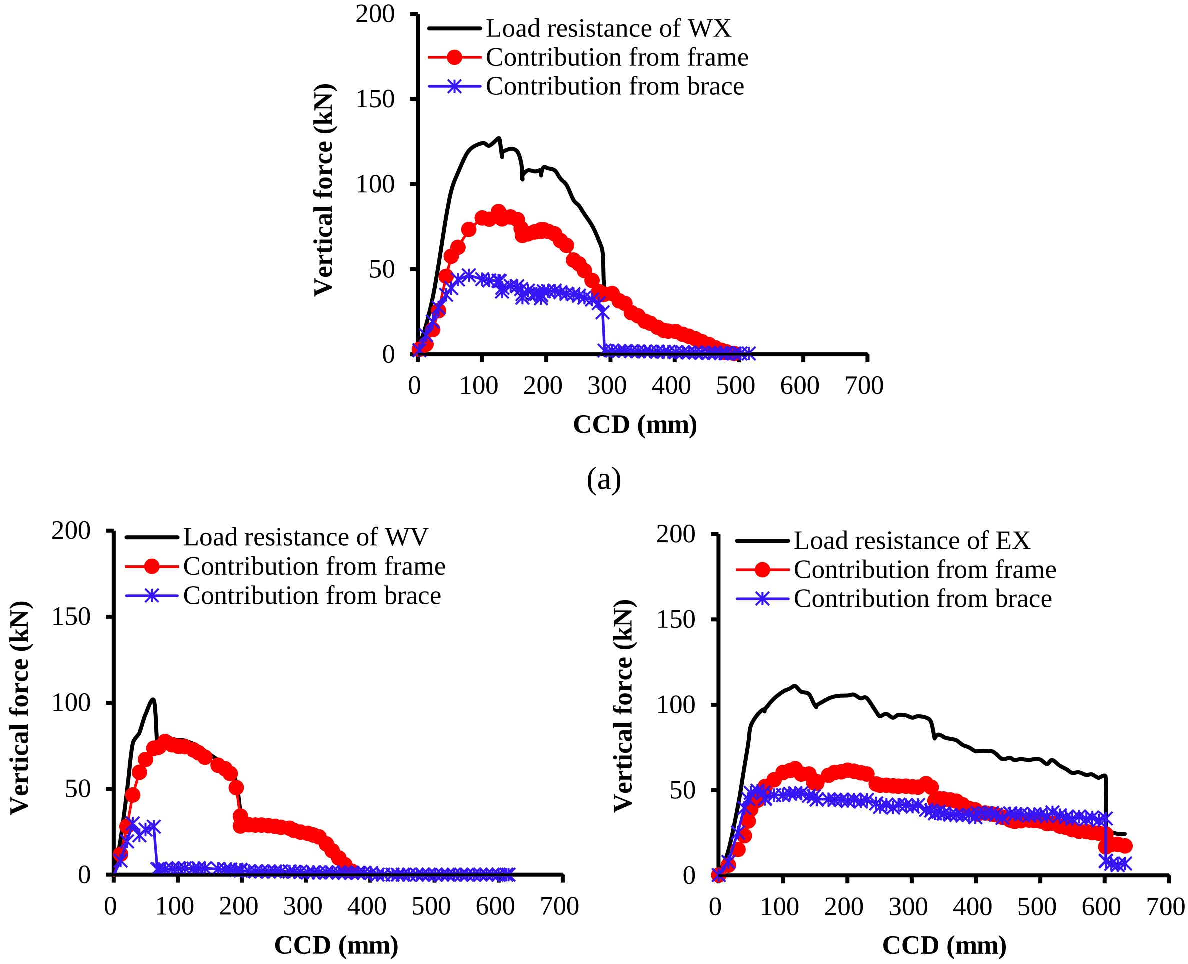

(b) (c)

Fig. 14. De-composition of the load bearing capacity from frame and braces

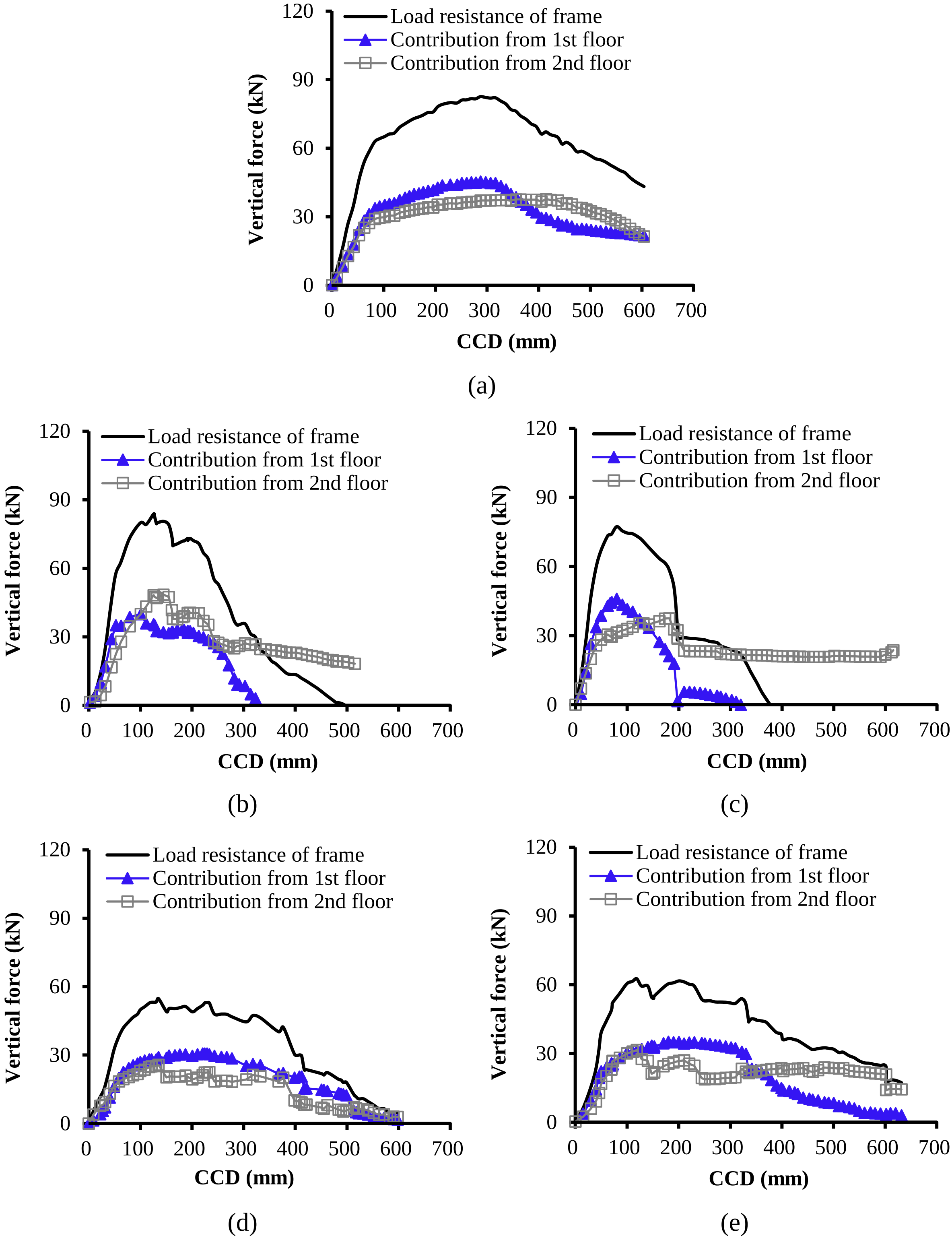

Fig. 15. De-composition of load bearing capacity from the 1st floor and 2nd floor

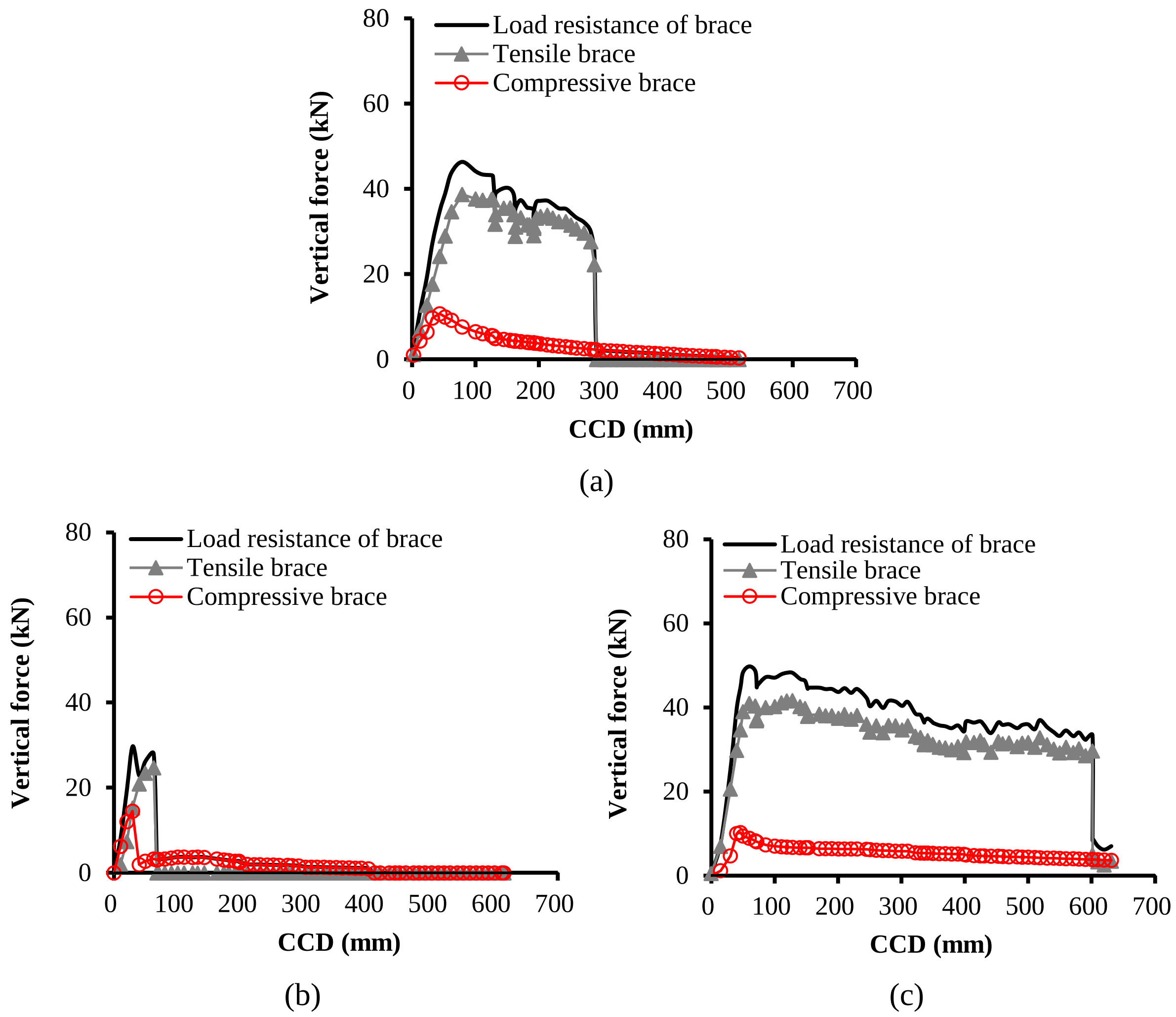

Fig. 16. De-composition of the load bearing capacity from tensile brace and compressive brace

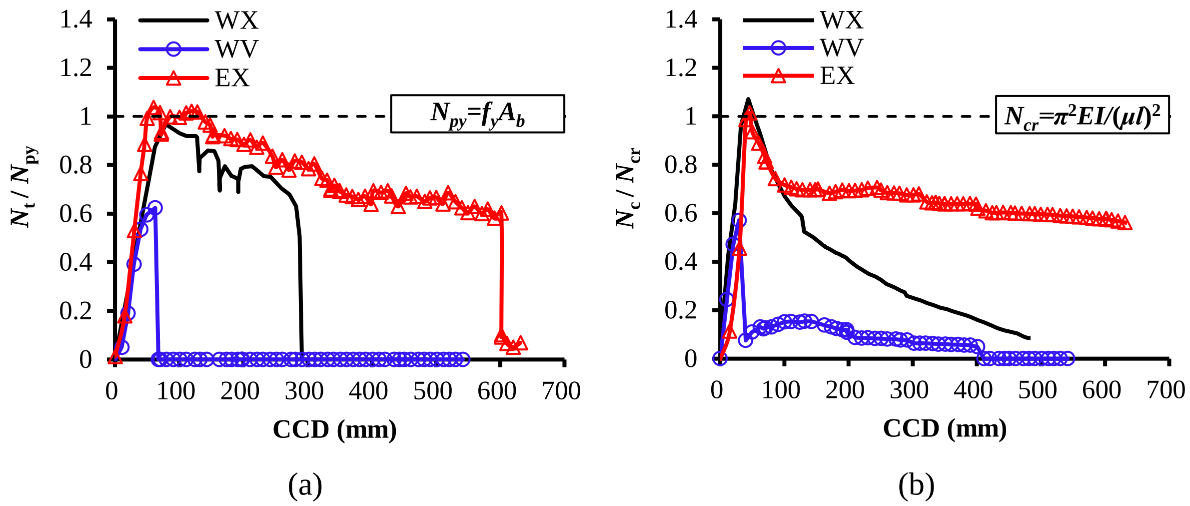

Fig. 17. Axial force of braces: (a) tensile brace; (b) compressive brace

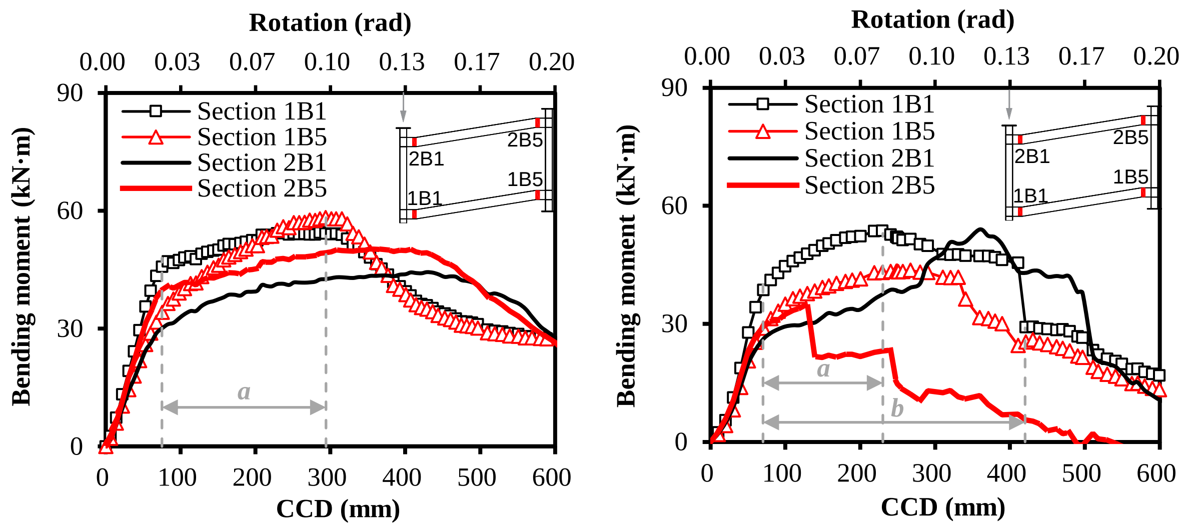

(a) (b)

Fig. 18. Bending moment development at the beam ends: (a) WB; (b) EB

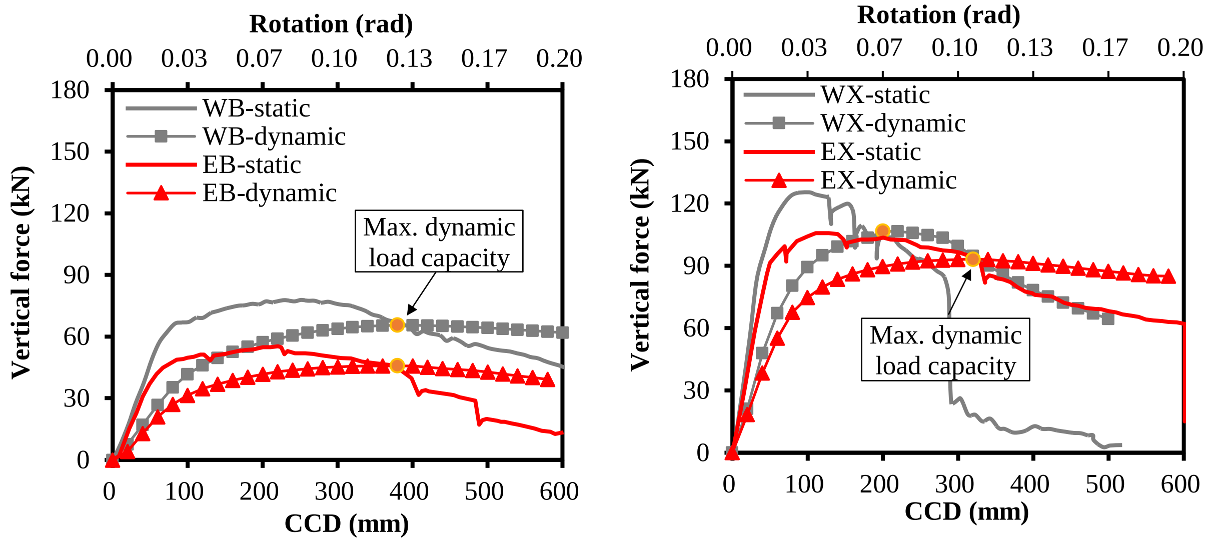

(a) (b)

Fig. 19. Comparison of the static and dynamic load resistance: (a) WB and EB; (b) WX and EX

Conflict of interest

The authors declare that there is no conflict of interest regarding the publication of this paper.

Corresponding Author: Kai Qian, qiankai@glut.edu.cn

Author Statements

Xi Lan: Writing- Original draft preparation; **Zhi Li:** Writing- Original draft preparation; **Feng Fu**: Reviewing and Editing; **Kai Qian**: Supervision.

Robustness of Steel Braced Frame to Resist Disproportionate Collapse Caused by Corner Column Removal

Xi Lan[1], Zhi Li[2], Feng Fu[3], Kai Qian[2*]

[1]College of Civil Engineering and Architecture, Guangxi University, Nanning, China, 530004.

[2]Guangxi Key Laboratory of New Energy and Building Energy Saving at Guilin University of Technology, China, 541004.

[3]Department of Engineering, School of Science and Technology at City, University of London, EC1V 0HB U.K.

Abstract:

Steel braces have been widely used as a major lateral stability system to resist the lateral load. However, the influences of steel braces on enhancing the load resistance in moment-resisting steel frames under column removal have not been studied adequately due to the lack of experimental data, especially under worst case scenarios, corner column removal. Thus, five two-floor steel moment-resisting subframes with or without braces were tested by applying a pushdown force. The purpose of this study is to quantify the effects of steel braces on the robustness of steel moment-resisting frames against disproportionate collapse. The test results indicated that steel braces could enhance the ultimate load bearing capacity up by 102.3 %. Compared to V configuration, X configuration is more efficient in increasing the load resistance since a proportion of the vertical load may be transferred to the side column through diagonal braces straightly. The de-composition of the load bearing capacity indicated that compressive braces only affect the initial stiffness and most of the load resistance is attributed to tensile braces for both X and V configurations. De-composition of the load bearing capacity indicated that the load bearing capacity from the first floor is normally greater than that from the second floor due to greater Vierendeel action mobilized.

Author Keywords: Disproportionate collapse; Corner column; Steel frame; Braces; Test

* Corresponding author. Professor, E-mail address: qiankai@glut.edu.cn

1. Introduction

Disproportionate collapse is an event, when the failure of the loss of one or a couple of members, results in the collapse of building disproportionate to the initial local failure. In recent years, the collapses of steel frames occurred frequently, including the landmark building twin towers, in New York in 2001, the steel frame at Xinjia Hotel building in Quanzhou, China in 2020, etc., which have received considerable attention from the public due to catastrophic consequences.

Potential hazards with abnormal load (i.e. vehicular impact, fire, gas explosion, and terrorist attack, etc.) may trigger disproportionate collapse [1-3]. Due to limited alternate load paths of the remaining structure, the removal of columns at corners is more vulnerable than other column missing scenarios. Kim and Kim [4] numerically evaluated the probability of disproportionate collapse of steel moment-resisting frames subjected to various column removal scenarios. They found that the vulnerability of disproportionate collapse was greatest when a corner. column was removed suddenly. Gerasidimis [5] investigated the disproportionate collapse vulnerability of steel frames for the case of a corner column loss and developed an analytical method to capture the collapse mechanism of a steel frame under corner column-removal scenarios. Based on numerical analysis, Fu and Tan [6] studied the disproportionate collapse mechanism of composite floor systems after a corner column was removed. Compared with the results obtained in the case of internal column removal, catenary action and tensile membrane action in beams failed to develop. These studies provided insight into the disproportionate collapse of steel frames after a corner column was removed behavior associated with the removal of corner columns from steel frames. However, other studies [7-12] found that the bending moments of the beam end near the corner joints reversed after the corner column was removed, leading to a significantly bending moment (the bottom subject to tension) developed there. Based on tests on singlefloor beam-column sub-assemblages, most existing studies [13-16] captured the performance of multi-floor steel frames under the scenario of a corner column removal by simplifying them as cantilever beams, which unrealistically ignored the interaction of structural members in different floors (Vierendeel action).

However, structures are not normally designed for the catastrophic consequences provoked by abnormal events. On the other hand, it is not economical to rehabilitate the structures just for the purpose of increasing disproportionate collapse resistance. Thus, design engineers should be aware of the potential vertical load resistance, which had been ignored in conventional design, such as the additional load resistance from masonry infilled walls and steel braces. Xavier et al. [17] tested a steel substructure incorporating infilled walls, which indicated that infilled walls affect the behavior of steel frames significantly. Moreover, Shan et al. [18] investigated the effect of infilled walls on the load resistance of the steel moment frames. They indicated that masonry infill walls could enhance the load bearing capacity and initial stiffness significantly. However, they will change the failure patterns. Seismic investigations had confirmed that the moment resisting frames with braces was an efficient seismic resisting system with sufficient lateral load resistance and stiffness [19, 20]. However, the ability of steel braces to improve the performance of steel frames to resist disproportionate collapse is still unclear. Khandelwal et al. [21] revealed that steel braced frames which were designed to meet seismic requirements could survive even if a column was removed suddenly, since the steel braces are effective in providing additional load resistance. It was found that horizontal braces could be employed to retrofit the steel moment-resisting frame [22]. It was indicated that an additional alternate load path was formed by horizontal braces, and thus, partial loads were directly transferred to the side columns.

However, experimental investigations of steel bracing systems after the removal of a corner column were rare. Moreover, the connections types in previous numerical studies are either pinned or fully restrained [23-25], the behavior of steel braced frames using partially restrained connections is still unclear. In this experimental program, five two-floor and two-bay steel moment-resisting frames were designed and tested after the removal of a corner column removal. The influence of different steel bracing configurations and connection types were quantified experimentally and analytically.

2. Experimental program

2.1. Test specimens

As listed in Table 1, five test specimens including three braced frames (WX, WV, and EX) and two bare frames without any braces (WB and EB), were designed in this experimental program. As the main investigated parameters were the connection types and bracing configuration, the specimens were labeled as follows: the alphabets “W” and “E” represent welded and end-plate connection, respectively. Then, the alphabet of “B”, “X”, and “V” stand for bare frames, braced frames with X-shaped bracing, braced frames with V-shaped bracings, respectively. Referring to Fig. 1, the prototype frame is designed according to ANSI/AISC 360-05 [20]. The prototype frames had 6×6 bays with a transverse and longitudinal span of 6.0 m and 8.4 m, respectively. The floor height is 3.0 m. The dead load and live load were 5.1 kN/m^2 and 3.0 kN/m^2, respectively. For braced frames, the prototype frame is seismic designed. Site class D was assumed and the critical acceleration parameters S_{DS} and S_{D1} are 0.20 and 0.14, respectively. For bare frames with non-seismic design, identical frames as the braced frames except no braces were installed for comparison. As illustrated in Fig. 1, a two-floor subframe was derived from the prototype frame as a specimen for testing. Considering the limitation of lab and facility, only half-scale sub-frames were tested.

In contrast to the corner column without additional horizontal restraints, overhanging beam (length of 655 mm) was fabricated beyond the side column to consider the horizontal constraints from the interior bays, which will connect with an A-frame by horizontal chain-poles (refer to Fig. 2a). The cross-section of beams and columns is HN 200×100×5.5×8 and HW 150×150×7×10, respectively. Fig. 3 presented the fabrication details of the specimens. For welded connection, complete joint penetration welds were used to connect the beams and columns. For end-plate connection, the beam was welded to an end plate with thickness of 10 mm. Eight M18 Grade 8.8 frictional bolts are employed for bolt connection with a pre-loading force of 345 N·m. The braces and the connections were designed based on ANSI/AISC 341-05 [19]. The braces and beams are connected by the gusset plates welded to the beam flanges. The uniform force method was employed to determine the force acting on welds [26]. To avoid the gusset plate premature yield and fracture occurred in the gusset plate before braces failure, the gusset plate is designed relatively stronger [19, 21]. Taking WX and EX as an example, the braces were made by steel angles with a dimension of 36 ×36 × 4 mm as shown in Fig. 2a. WX and EX have X shaped braces and the size of gusset plate is 330×125×12 mm. In addition, WV has V shaped braces. The gusset plates installed in the second floor have a size of 160×155×12 mm while the gusset plate installed in the first floor has a size of 510×155×12 mm.

2.2. Material properties

All structural members were fabricated by Grade Q235 steel. As displayed in Table 2, the critical material properties of each component are measured via coupon tests in accordance with the relevant specification [27]. The average value of three coupons was calculated for each set of results in this table. The properties of M18bolts were provided by supplier.

2.3. Test setup

As illustrated in Fig. 4a, the ground corner column was not assembled to represent the initial damage. Beneath each side column, a pin support was applied. The vertical load was imposed at the top of corner column through a whisky jack. Displacement-controlled loading method was adopted. At the beginning of the test, a loading rate of 5 mm/min was set until reaching the vertical displacement of 100 mm. In the subsequent loading process, the loading rate of 10 mm/min was adopted. The applied concentrated load was monitored by a load cell, which was placed beneath the whisky jack. To prevent undesirable out-of-plane failure, a steel assemblage was specially arranged.

To represent the axial loads from upper floors, a whisky jack was applied on the side column to guarantee an axial compressive ratio of 0.3. The overhanging girder, if any, was connected to the reaction frame through a horizontal chain-pole. Tensile/compressive load cell was mounted in the horizontal chain-pole, so that the horizontal reaction force could be monitored. To measure the vertical load redistribution to the side column, each pin support was installed a load pin. Above the corner column, a hinge was set to allow the conceivable rotation of the corner column during the test. Moreover, two transverse beams with rollers were mounted at both sides of the corner column to prevent out-of-plane movement during the test. In addition, as shown in Fig. 4a, three LVDTs were mounted along the beam of first floor in the corner bay. It should be mentioned that the deflection of beam between side columns was negligible during the test of Specimen WB, thus they were not monitored in the following tests. As given in Fig. 2, to determine the variations of the axial forces and bending moments in the beams, a series of strain gauges were attached to the critical sections.

3. Test results

In order to assess the robustness of steel bending-moment frames with steel braces, five two-floor steel sub-frames with or without bracings were experimentally tested after a corner column loss. The key results are tabulated in Table 3 and presented below.

3.1 Global behavior

WB: The load-displacement curves at the corner column of WB, WX, and WV are displayed in Fig. 5. The specimens initially exhibited elastically as the load resistance increased linearly. The yield load was measured to 64.7 kN at the corner column deflection (CCD) increased to 80 mm. Thus, it has initial stiffness of 0.8 kN/mm. The initial stiffness was defined as the ratio of yield load to yield displacement herein. The load resistance started to decrease after the occurrence of local buckling at beam flanges in the first floor, which was attributed to the effects of flexural bending. At an CCD of 233 mm, the ultimate load bearing capacity, which was defined as the peak load resistance, of 78.2 kN was reached. On further increasing the displacement, similar local buckling also occurred at beam flanges in the second floor at CCD of 400 mm. Fig. 6 shows the failure pattern of the specimen. Although no fracture occurred during the test, the local buckling was severe at the beam ends, which resulted in the beam of the first floor failing in torsion in absence of catenary action.

WX: As the second floor has X braces, the failure pattern of WX was changed. In the start of testing, the compressive braces started to buckle, which indirectly showed that the compressive braces may have little contribution to the load enhancement. This can be confirmed by the strain gauge results later. As displayed in Fig. 5, it has a yield load of 116.5 kN at an CCD of 62 mm. Moreover, it has initial stiffness of 1.9 kN/mm, about 232.3% of that of WB. Similar to WB, local buckling of the bottom beam flange occurred near the side column in the ground floor at this stage. It has an ultimate load bearing capacity of 125.4kN. The tensile brace fractured at an CCD of 288 mm, which leads to the load resistance dramatically dropping from 74.9 kN to 24.3 kN. Fig. 7 gives the failure pattern of the specimen. Tensile braces were fractured and compressive braces were severely buckled. No yielding was observed in the gusset plates. Similar to WB, torsional damage occurred in the beam in the first floor. However, premature weld fractures occurred in Joints S1, S2 and C2 of WX, which were not observed in WB. This was due to the additional shear forces from the steel braces and the torsion-induced shear forces in the beams.

WV: For WV, it has a yield load of 93.5 kN and initial stiffness of 1.9 kN/mm. Similar to WX, the compressive braces began to out-of-plane buckling at the very beginning of the load. Different from WX, the tensile brace fractured at a relatively early stage (corresponding to CCD of 63 mm) and followed by the drop in load resistance dramatically. Moreover, it has an ultimate load bearing capacity of 100.9 kN, which is 129.0% and 80.5% of that of WB and WX, respectively. When the fracture occurred at the beam ends, the load resistance dropped significantly. After reaching the CCD of 191 mm, the load bearing capacity of WV became even lower than that of WB. Fig. 8 displays the failure pattern of WV. Similar to WX, the compressive braces suffered severe buckling and the tensile braces were fractured. However, different from WX, there is no torsional damage occurring in the beams with gusset plate welded to the beam flange were enough to prevent torsional buckling.

EB: Fig. 9 compares the load-displacement curves of EB and EX. EB achieved a yield load of 42.7 kN and initial stiffness of 0.7 kN/mm. When the CCD reached 135 mm, the welds nearby the side column in the second floor fractured. Subsequently, the load bearing capacity could increase until further weld fracture occurred at the end-plate. It has an ultimate load bearing capacity of 55.5 kN. Similar fractures occurred at the beam ends near the corner column at CCD of 406 mm and 487 mm, respectively. Fig. 10 gives the failure pattern of the specimen. The failure of EB was controlled by weld failure at the end-plate.

EX: It has a yield load of 86.4 kN and initial stiffness of 1.9 kN/mm. The weld fracture was initially developed nearby the corner column. With the displacement kept increasing to 128mm, EX reached its ultimate load bearing capacity of 105.8 kN. When CCD increased to 159 mm and 336 mm, the welds fracture was formed at the beam ends in sequence. The tensile braces fractured at an CCD of 602 mm, which was 109.0% later than WX. Fig. 11 gives the failure pattern of EX. Similarly, the compressive brace suffered severe out-of-plane buckling while the tensile brace fractured. Moreover, local buckling occurred at point A.

3.2 Deformation measurements

The deformation shape of beams at different stages is displayed in Fig. 12. Following DoD [28], the chord rotation was defined as the ratio of CCD to beam span. From the figure, the chord rotation would significantly underestimate the rotation of the beam end nearby the corner column. On the other hand, the chord rotation could assess the rotation of the beam end nearby the side column accurately, especially for WX and WV. The external steel brace would not significantly change the deflection shape of the beams. Similar observation was achieved in EB and EX.

3.3 Internal force evaluation

To deeply understand the contribution of load resistance from braces, the contribution of braces and frames should be determined individually. Before that, the reliability of calculation formula to determine the internal force of each component based on strain gauge results must be verified. From Fig. 2a, Sections B1-4 installed a series of strain gauges, which could help to determine the internal force. Similar to the calculation method proposed in the previous paper [29, 30], the load-displacement curve based on strain gauge data was determined and compared with the one from load cell results (refer to Fig. 13). As shown in Fig. 13, good agreements are achieved between the one measured by the load cell and analytical results from strain gauge data. For WX and EX, the minor discrepancy of initial stiffness may be caused by unavoidable gaps in the test setup, which did not reflect in the LVDT placed above the corner column. Generally, the analytical results based on strain gauges can well capture the character of the curve until failure.

Fig. 14 presents the load bearing capacity of the braces and frame. Relying on the analytical results of internal force, it was revealed that the load bearing capacity from the bare frame was purely provided by flexural action, the contribution of catenary action could be ignored due to the limited tensile forces in the beams. For WX, at the ultimate load resistance stage, the contribution of steel braces was about 35.3%. With the increasing vertical displacement, the load resistance of the steel braces began to decrease due to the yield of beam section releasing the constraints for the tensile braces gradually. For WV, at the stage of ultimate load bearing capacity, the contribution of steel bracing was only 27.7% as the tensile braces fractured. Different from the braced frames with welded connection, for EX, initially, the steel braces contributed greater load resistance than the frame. At the stage of ultimate load resistance, the contribution of steel braces was 45.7%, which was comparable to that of the frame. Moreover, after that, the load resistance from braces is always comparable to that from frames until the test final.

4. Discussion of experimental results

4.1 Contribution of load resistance

The de-composition of the frame contribution from each floor is given in Fig. 15. As shown in the figures, the load bearing capacity from the first and second floor has similar trends until failure occurred in the connections, while the first floor has slightly greater load resistance than that of second floor. This was due to the greater rotational constraints and Vierendeel action, for which further explanation would be in section 4.2. However, WX had a greater maximum load resistance from the second floor as the connection in the first floor fractured earlier.

Fig. 16 displays the de-composition of load bearing capacity contribution from tensile brace and compressive brace. For WB, WX, and WV, the maximum load resistance from steel braces was 46.4, 29.7, and 49.8 kN, respectively. Different from WX and EX, which reached their maximum load resistance until the tensile brace yielded, the maximum load resistance of WV was obtained when the compressive brace buckled. For WV, the compressive brace contributed the maximum load resistance of 14.5 kN, which was 33.7% and 41.2% higher than that of WX and EX, respectively. To better understand the contribution of steel braces, the development of axial force of tensile brace and compressive brace was normalized, as shown in Fig. 17. The tensile brace has an analytical yield load of 85.6 kN. And the compressive brace has buckling loads of 23.0 kN and 57.6 kN for X and V configuration, respectively. As can be seen in the figure, both the tensile and compressive brace in X configuration achieved their yield and buckling loads. However, in V configuration, the tensile brace could not achieve the analytical yield load and the compressive brace could not reach the analytical buckling load as the constraints applied at the braces of V configuration were not translation fixed, which is assumed in analytical analysis.

4.2 Effects of connection types

Unlike braced frames where the maximum deformation would be introduced by the failure of the steel bracing, the maximum deformation of bare frames difficult to identify from the load-displacement curve. The deformation capacities of bare frame were defined as vertical displacement at ultimate load bearing capacity. For WB and EB, the maximum deformation was 233 and 228 mm, respectively. Thus, WB and EB had a similar maximum deformation, which was quite different from the case of missing a middle column [29, 30]. WB was able to sustain large deformation caused by the torsion developed in beams, and avoided the brittle weld fracture. Fig. 18 shows the development of bending moments at the beam ends. From the figure, not only the beam end near the side column, the beam end near the corner column also experienced large positive bending moments, which was different from the behavior of unsupported cantilevers. This indicated that Vierendeel action played an important role in the load resisting mechanism after corner column removal. Moreover, DoD [28] defined the acceptable plastic rotation angles for different type of steel connections. Taking Section 1B1 as an example, the parameters ‘a’ and ‘b’ were defined as shown in Fig. 18. Table 4 compared the measured parameters with the requirements in specification, which showed that the recommended ductility acceptance criteria were conservative for both fully and partially restrained moment connections in current specimens.

Although this experimental test was focused on the static performance of welded and endplate connections, disproportionate collapse following sudden column removal exhibits a typical dynamic response. Based on the available static load-displacement curve, a dynamic capacity evaluation was applied using an energy-based method proposed by Izzuddin et al. [31]. This approach has been applied and verified in previous studies related to disproportionate collapse [32-34]. As described in Eq. (1), the equivalence between external work (dynamic response) and internal energy (static response) was used to obtain the dynamic response shown in Fig. 19.

$$P_d\left(u_d\right)=\frac{1}{u_d}\int_0^{u_d} P_{NS}(u)du \tag{1}$$

As labeled in Fig. 19, the maximum dynamic load capacities of WB, EB, WX, and EX were 65.5, 45.8, 106.7, and 93.2 kN, respectively. Prior to this point being reached, it was unlikely for the specimens to undergo disproportionate collapse even if a sudden column failure occurred. The maximum dynamic deformations of WB, WX and WV were 380, 380, 200 and 320 mm, which were 163%, 194%, 167% and 250% of that of maximum static deformations, respectively. This implied that the deformation capacity of the frames under sudden column removal were greater than those under quasi-static loading for the same applied load.

4.3 Effects of braces types

As seen from Fig. 5, the yield load of WB, WX, and WV were 64.7, 116.5 and 93.5 kN, respectively. Therefore, the X and V braces enhanced the yield load of WB by 80.1% and 44.5%, respectively as the X bracing configuration in WB can directly transfer a portion of the load to the side column. Regarding the ultimate load bearing capacity, WB, WX and WV were 78.2, 125.4 and 100.9 kN, respectively. Therefore, the X and V bracing configuration enhanced the ultimate load bearing capacity of WB by 60.4% and 29.0%, respectively. This could be attributed into the tensile braces in V configuration fractured much earlier, even earlier than the yielding of the beams. Moreover, the maximum deformation of WB, WX and WV were 233, 288 and 63mm, respectively. Thus, the steel bracing with X configuration increased the maximum deformation of WB by 23.6%, while the steel bracing with V configuration decreased the maximum deformation of WB by 73.0%. The maximum deformation of WX was 457.1% of that of WV. Regarding to failure patterns, as shown in Fig.12, torsional damage occurred at interfaces between the beam and corner column joint of WB and WX [35, 36]. However, due to the gusset plate of V bracing configuration, the critical beam section shifted close to the beam midspan, which prevented the torsional damage of WV [37].

5. Conclusions

A series of five two-bay and two-floor steel sub-frames were tested subjected to a corner column missing scenario to investigate the robustness of steel braced frames to resist disproportionate collapse. Following conclusions are obtained:

1. Steel braces could increase the initial stiffness and load resistance of steel frames whatever X configuration or V configuration was adopted. However, torsion may control the failure of bare frame, while the braces also amplified the shear force demand at the beam ends. Therefore, it is necessary to consider the torsional shear forces of adjacent structures where corner column is removed in the alternate load path method. The connection design can be controlled by the shear forces generated by torsion, especially for braced frame.
2. Experimental results indicated that the tensile braces in steel frames with end-plate connections did not fracture until the vertical deformation reached 20% of the beam span. X configuration performed better than V configuration regarding ultimate load bearing capacity and initial stiffness, as X configurations could transfer partial of the load to the side column directly while V configuration are only subjected to axial forces within the elastic range. Whatever X or V configurations, the compressive braces only affect the initial stiffness as they were severely buckled from the very early beginning of the test.
3. Different from the scenario of loss of an interior column, the bare frame with weld connection achieved a similar maximum deformation than that of steel frame with end-plate connections when the scenario of corner column missing was concerned. Moreover, the value of plastic hinge properties was too conservative for the bare frame with weld connection and end-plate connection under corner column removal.
4. Analytical analysis found that the load resistance of the frame in the ground floor is generally larger than that in the second floor because the structural components in the second floor could provide horizontal constraints to the joints in the ground floor, in other words, greater Vierendeel action was mobilized in the frames in the ground floor.

Acknowledgements

The authors gratefully acknowledge the financial support provided by the National Natural Science Foundation of China (Nos. U22A20244 and 52022024) and Natural Science Foundation of Guangxi (No.2021GXNSFFA196001). Any opinions, findings and conclusions expressed in this paper do not necessary reflect the view of National Natural Science Foundation of China and Natural Science Foundation of Guangxi.

References

[1] B.R. Ellingwood, R. Smilowitz, D.O. Dusenberry, D. Duthinh, H. Lew, N.J. Carino, Best practices for reducing the potential for progressive collapse in buildings, National Institute of Standards and Technology, Gaithersburg, Maryland, U.S.A. (2007).

[2] D.C. Feng, M.X. Zhang, E. Brunesi, F. Parisi, Y. Jun, Z. Zhen, Investigation of 3D effects on dynamic progressive collapse resistance of RC structures considering slabs and infill walls, J. Build. Eng. 54(15) (2022) 104421. https://doi.org/10.1016/j.jobe.2022.104421.

[3] I.M.H. Alshaikh, B.H.A. Bakar, E.A.H. Alwesabi, A.A. Abadel, H. Alghamdi, A. Altheeb, R. Tuladhar, Progressive collapse behavior of steel fiber-reinforced rubberized concrete frames, J. Build. Eng. (2022) 104920. https://doi.org/10.1016/j.jobe.2022.104920.

[4] J. Kim, T. Kim, Assessment of progressive collapse-resisting capacity of steel moment frames, J. Constr. Steel Res. 65(1) (2009) 169-179. https://doi.org/10.1016/j.jcsr.2008.03.020.

[5] S. Gerasimidis, Analytical assessment of steel frames progressive collapse vulnerability to corner column loss, J. Constr. Steel Res. 95 (2014) 1-9. https://doi.org/10.1016/j.jcsr.2013.11.012.

[6] Q. N. Fu, Tan, K. H, Numerical study on steel-concrete composite floor systems under corner column removal scenario, Structures. 21, (2019) 33-44. https://doi.org/10.1016/j.istruc.2019.06.003.

[7] M. Sasani, S. Sagiroglu, Progressive collapse resistance of Hotel San Diego, J. Struct. Eng. 134(3) (2008) 478-488. https://doi.org/10.1061/(ASCE)0733-9445(2008)134:3(478).

[8] I. Azim, J. Yang, S. Bhatta, F.L. Wang, Q.F. Liu, Factors influencing the progressive collapse resistance of RC frame structures, J. Build. Eng. 27 (2022) 100986. https://doi.org/10.1016/j.jobe.2019.100986

[9] K. Qian, B. Li, Z. Zhang, Influence of multicolumn removal on the behavior of RC floors, J. Struct. Eng. 142 (2016) 04016006. https://doi.org/10.1061/(ASCE)ST.1943-541X.0001461.

[10] A.T. Pham, N.S. Lim, K.H. Tan, Investigations of tensile membrane action in beam-slab systems under progressive collapse subject to different loading configurations and boundary conditions, Eng. Struct. 150 (2017) 520-536. https://doi.org/10.1016/j.engstruct.2017.07.060.

[11] J. Z. Zhang, B. Jiang, R. Feng, R. Chen, Robustness of steel moment frames in multi-column-removal scenarios, J. Constr. Steel Res. 175, (2020) 106325. https://doi.org/10.1016/j.jcsr.2020.106325.

[12] K. Qian, X. Lan, Z. Li, F. Fu, Behavior of steel moment frames using top-and-seat angle connections under various column removal scenarios, J. Struct. Eng. 147 (10) (2021) 04021144. https://doi.org/10.1061/(ASCE)ST.1943-541X.0003089.

[13] W. Wang, J.J. Wang, X. Sun, Y.H. Bao, Slab effect of composite subassemblies under a column removal scenario, J. Constr. Steel Res. 129(2) (2017) 141-155. https://doi.org/10.1016/j.jcsr.2016.11.008.

[14] P.M. Stylianidis, D.A. Nethercot, B.A. Izzuddin, A.Y. Elghazouli, Study of the mechanics of progressive collapse with simplified beam models, Eng. Struct. 117 (2016) 287-304. https://doi.org/10.1016/j.engstruct.2016.02.056.

[15] J. Hou, L. Song, H.H. Liu, Testing and analysis on progressive collapse-resistance behavior of RC frame substructures under a side column removal scenario, J. Perform. Constr. Facil. 30(5) (2016) 04016022. https://doi.org/10.1061/(ASCE)CF.1943-5509.0000873.

[16] O. A. Mohamed, Assessment of progressive collapse potential in corner floor panels of reinforced concrete buildings, Eng. Struct. 31(3) (2009) 749-757. https://doi.org/10.1016/j.engstruct.2008.11.020.

[17] F.B. Xavier, L. Macorini, B.A. Izzuddin, C. Chisari, N. Gattesco, S. Noe, C. Amadio, Pushdown tests on masonry infilled frames for assessment of building robustness, J. Struct. Eng. 143(9) (2017) 04017088. https://doi.org/10.1061/(ASCE)ST.1943-541X.0001777.

[18] S.D. Shan, S. Li, S.H. Wang, Effect of infill walls on mechanisms of steel frames against progressive collapse, J. Constr. Steel Res. 162 (2019) 105720. https://doi.org/10.1016/j.jcsr.2019.105720.

[19] American Institute of Steel Construction, Seismic Provisions for Structural Steel Buildings, ANSI/AISC 341-05, Chicago, Illinois, U.S.A. (2005).

[20] American Institute of Steel Construction, Specifications for Structural Steel Buildings, ANSI/AISC 360-05, Chicago, Illinois, U.S.A. (2005).

[21] K. Khandelwal, S. El-Tawil, F. Sadek, Progressive collapse analysis of seismically designed steel braced frames, J. Constr. Steel Res. 65(3) (2009) 699-708. https://doi.org/10.1016/j.jcsr.2008.02.007.

[22] J. Chen, W. Peng, R. Ma, Strengthening of horizontal bracing on progressive collapse resistance of multistory steel moment frame, J. Perform. Constr. Facil. 26 (2012) 720-724. https://doi.org/10.1061/(ASCE)CF.1943-5509.0000261.

[23] J. Jiang, G. Q. Li, A, Usmani, Progressive collapse resistance of braced steel frames exposed to fire, Proceedings of the international conference on sustainable development of critical infrastructure (CDRM 8), Shanghai, China, May (2014).

[24] J. Kim, Y. Lee, H. Choi, Progressive collapse resisting capacity of braced frames, Struct. Des. Tall Spec. 20 (2011) 257-270. https://doi.org/10.1002/tal.574.

[25] B. Asgarian, F. H. Rezvani, Progressive collapse analysis of concentrically braced frames through EPCA algorithm, J. Constr. Steel Res. 70 (2012) 127-136. https://doi.org/10.1016/j.jcsr.2011.10.022.

[26] R.M. Richard, Analysis of large bracing connection designs for heavy construction, Proceedings of the 38th AISC National Engineering Conference, Chicago, Illinois, U.S.A, December. (1986).

[27] American Society for Testing and Materials (ASTM), Standard Test Methods and Definitions for Mechanical Testing of Steel Products, ASTM Standard A370-02, Philadelphia, PA (2002).

[28] DoD, Design of Building to Resist Progressive Collapse (UFC 4-023-03), Department of Defense, Washington D.C., U.S.A. (2009)

[29] K. Qian, X. Lan, Z. Li, Y. Li, F. Fu, Progressive collapse resistance of two-storey seismic configured steel sub-frames using welded connections, J. Constr. Steel Res. 170 (2020) 106117. https://doi.org/10.1016/j.jcsr.2020.106117.

[30] K. Qian, X. Lan, Z. Li, F. Fu, Effects of steel braces on robustness of steel frames against progressive collapse, J. Struct. Eng. 147 (11) (2021) 04021180. https://doi.org/10.1061/(ASCE)ST.1943-541X.0003161.

[31] B.A. Izzuddin, A.G. Vlassis, A.Y. Elghazouli, D.A.Nethercot, Progressive collapse of multi-storey buildings due to sudden column loss-Part I: simplified assessment framework, Eng. Struct. 30(5) (2008) 1308-1318. https://doi.org/10.1016/j.engstruct.2007.07.011

[32] Y.H. Weng, K. Qian, F. Fu, Q. Fang, Numerical investigation on load redistribution capacity of flat slab substructures to resist progressive collapse, J. Build. Eng. 29 (2020) 101109. https://doi.org/10.1016/j.jobe.2019.101109

[33] Y.H. Weng, F. Fu, K. Qian, Punching shear resistance of corroded slab-column connections subjected to eccentric load, J. Struc. Eng. 159(1) (2023) 04022219. https://doi.org/10.1061/(ASCE)ST.1943-541X.0003504

[34] K. Qian, B. Li, Effects of masonry infill wall on the performance of RC frames to resist progressive collapse, J. Struct. Eng. 143(9) (2017) 04017118. https://doi.org/10.1061/(ASCE)ST.1943-541X.0001860

[35] A. E. Mcmullen, B. V. Rangan, Pure tension in rectangular sections - a Re-examination, ACI Journal. 75(10) (1978) 511-519. https://doi.org/10.14359/10963.

[36] K. N. Rahal, M. P Collins, Analysis of sections subjected to combined shear and torsion-a Theoretical model, ACI Struct. J. 92(4), (1995) 459-469. https://doi.org/10.14359/995.

[37] A. T. Pham, D. P. Xuan, K. H. Tan, Slab-corner effect on torsional behaviour of perimeter beams under missing column scenario, Mag. Concrete Res. 71(12) (2018) 1-43. https://doi.org/10.1680/jmacr.18.00011.

Table 1. Summary of specimen

Specimen ID	Connection	Bracing configurations
WB	Welded	N/A
WX	Welded	X-shaped braces
WV	Welded	V-shaped braces
EB	End-plate	N/A
EX	End-plate	X-shaped braces

Table 2. Material properties

Items	Plate thickness (mm)	Yield strength (MPa)	Yield strain	Ultimate strength (MPa)	Ultimate strain	Elongation (%)
Beam flange	8	310	0.0019	420	0.024	12
Beam web	5.5	320	0.0021	430	0.0249	13.5
Column flange	10	300	0.0019	410	0.0267	14
Column web	7	295	0.0023	375	0.0242	13
Steel brace	4	310	0.0021	420	0.0256	12.5

Table 3. Test results

Test ID	U_{YL} (mm)	F_{YL} (kN)	K_{YL} (kN/mm)	U_{PL} (mm)	F_{PL} (kN)
WB	80	64.7	0.8	233	78.2
WX	62	116.5	1.9	103	125.4

WV	49	93.5	1.9	63	100.9
EB	60	42.7	0.7	228	55.5
EX	46	86.4	1.9	128	105.8

Note: F_{YL} and F_{PL} represent yield load and ultimate load bearing capacity, respectively; U_{YL} and U_{PL} represent displacements corresponding the yield load and ultimate load bearing capacity, respectively; K_{YL} represents initial stiffness corresponding the yield load.

Table 4. Comparison of the measured and recommended plastic hinge parameters in DoD [28]

Test ID	Section	'a' at the beam end (rad)	'a' in DoD [28] (rad)	'b' at the beam end (rad)	'b' in DoD [28] (rad)
WB	1B1	0.070	0.025	N/A	0.038
	1B5	0.073	0.025	N/A	0.038
	2B1	0.118	0.025	N/A	0.038
	2B5	0.093	0.025	N/A	0.038
EB	1B1	0.050	0.012	0.109	0.018
	1B5	0.063	0.012	0.084	0.018
	2B1	0.094	0.012	0.136	0.018
	2B5	0.026	0.012	0.061	0.018

List of Figures

Fig. 14. De-composition of the load bearing capacity from frame and braces

Fig. 15. De-composition of load bearing capacity from the 1st floor and 2nd floor

Fig. 16. De-composition of the load bearing capacity from tensile brace and compressive brace

Fig. 17. Axial force of braces: (a) tensile brace; (b) compressive brace

Fig. 18. Bending moment development at the beam ends: (a) WB; (b) EB

Fig. 19. Comparison of the static and dynamic load resistance: (a) WB and EB; (b) WX and EX

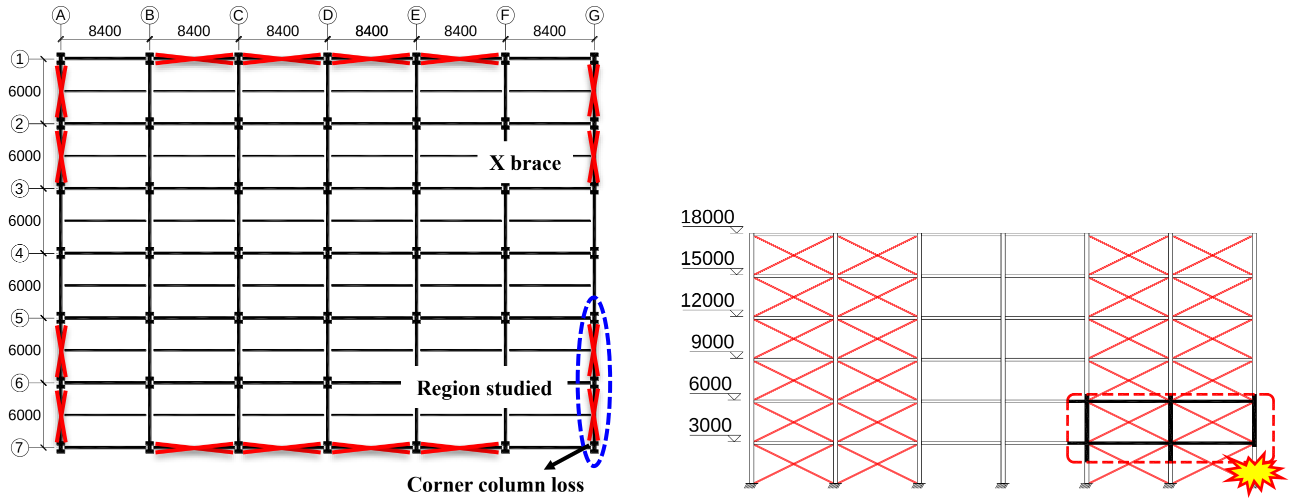

(a) (b)

Fig. 1. Prototype building and extracted frame (unit in mm): (a) front view; (b) side view

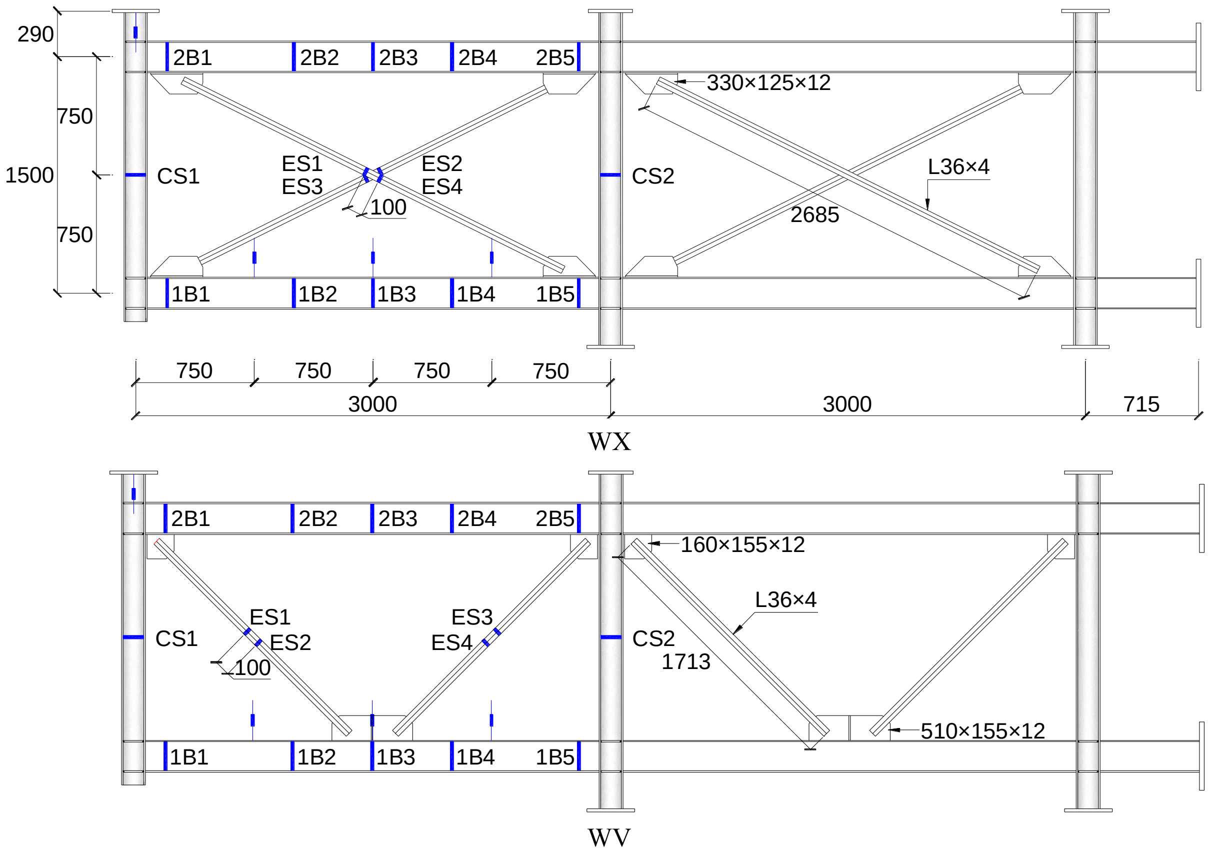

(a)

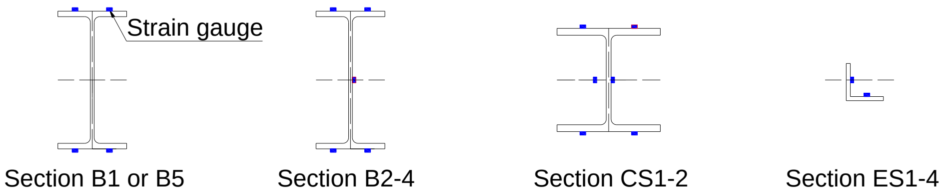

(b)

Fig. 2. Dimensions of the specimen and locations of instrumentations: (a) layout of strain gauge and displacement transducer; (b) position of strain gauges on sections

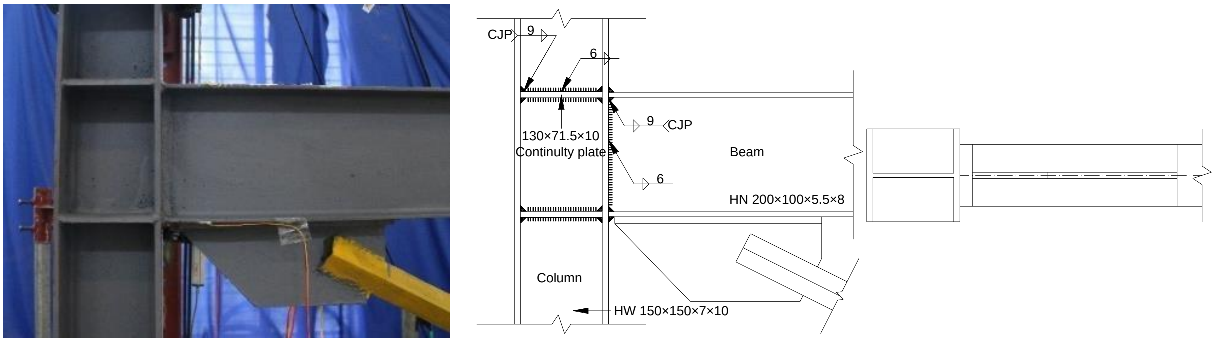

(a)

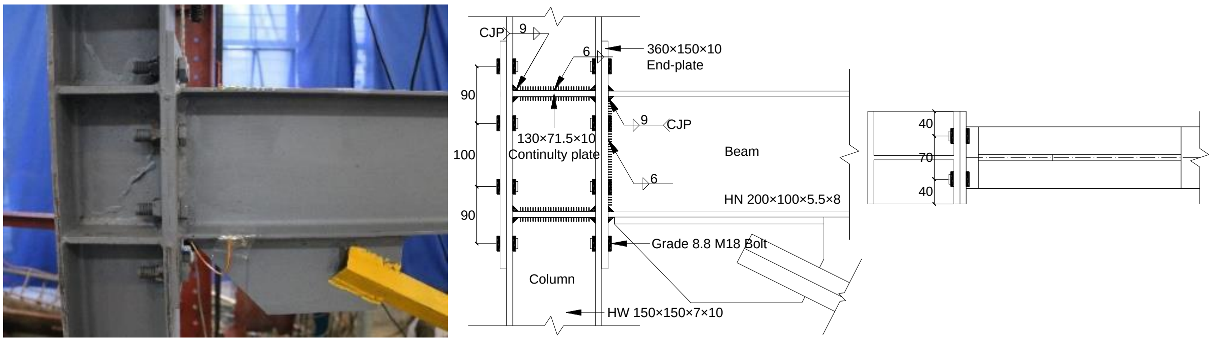

(b)

Fig. 3. Details of the connections: (a) welded connection; (b) end-plate connection

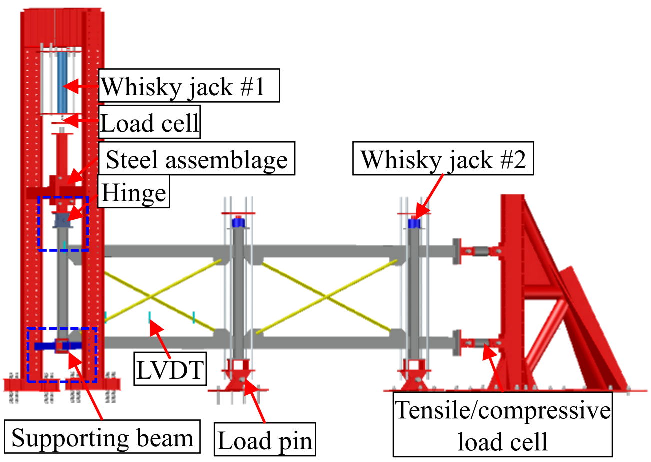

(a)

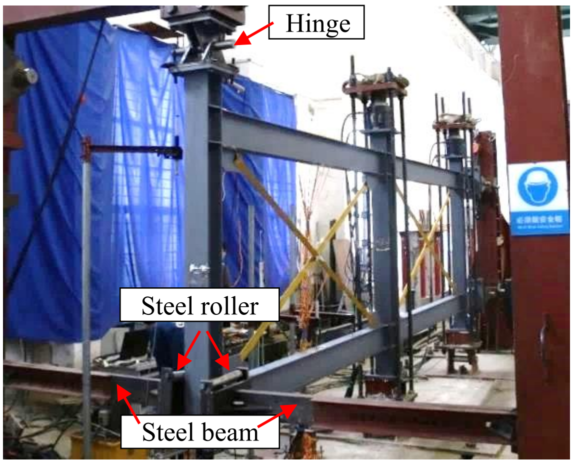

(b)

Fig. 4. Test setups of WX: (a) drawing; (b) photo

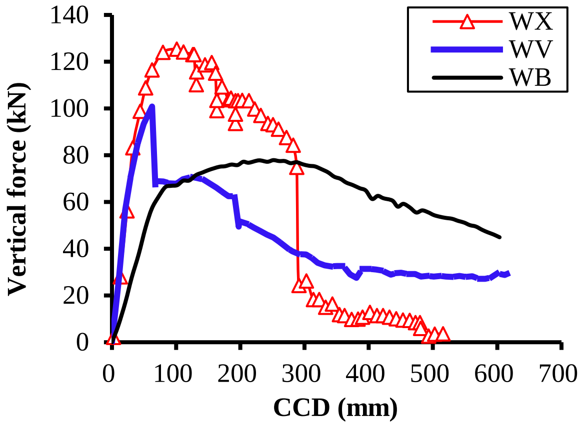

Fig. 5. Load-displacement curves of specimens: WB, WX and WV

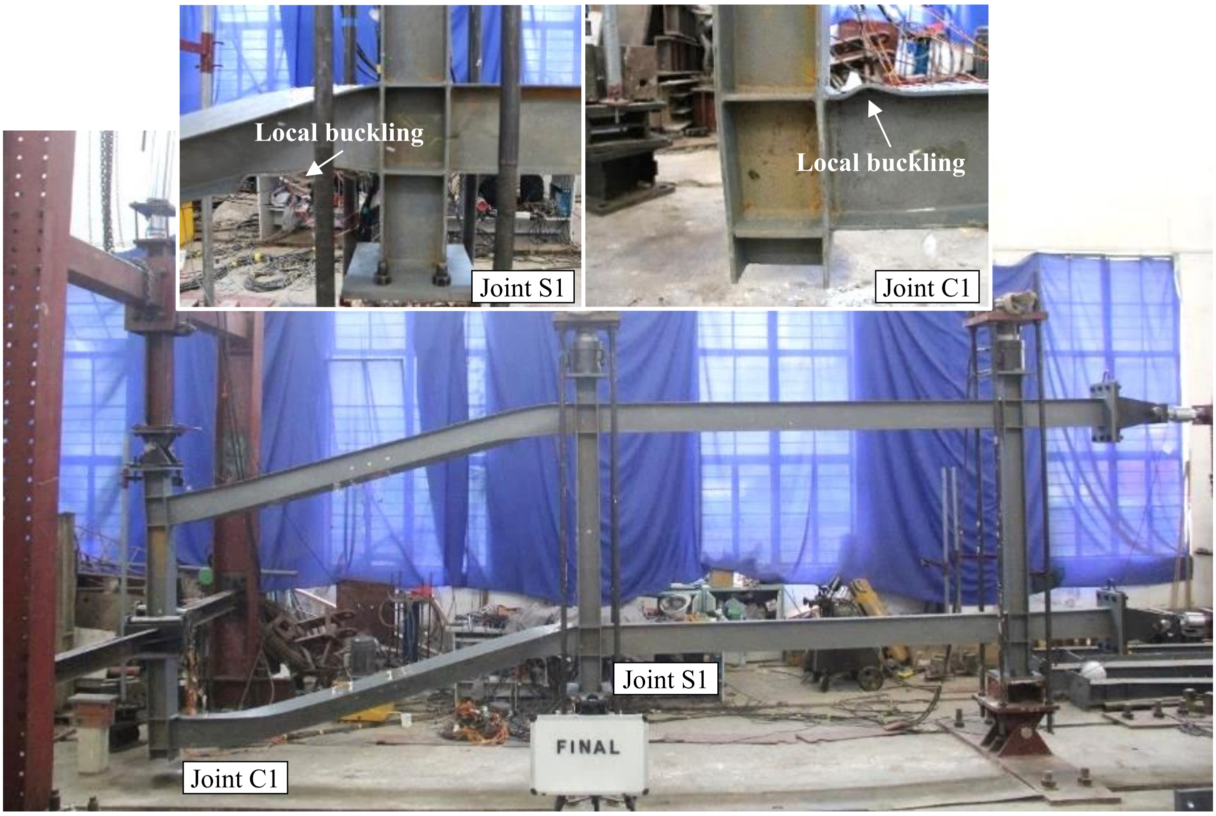

Fig. 6. Failure pattern of Specimen WB

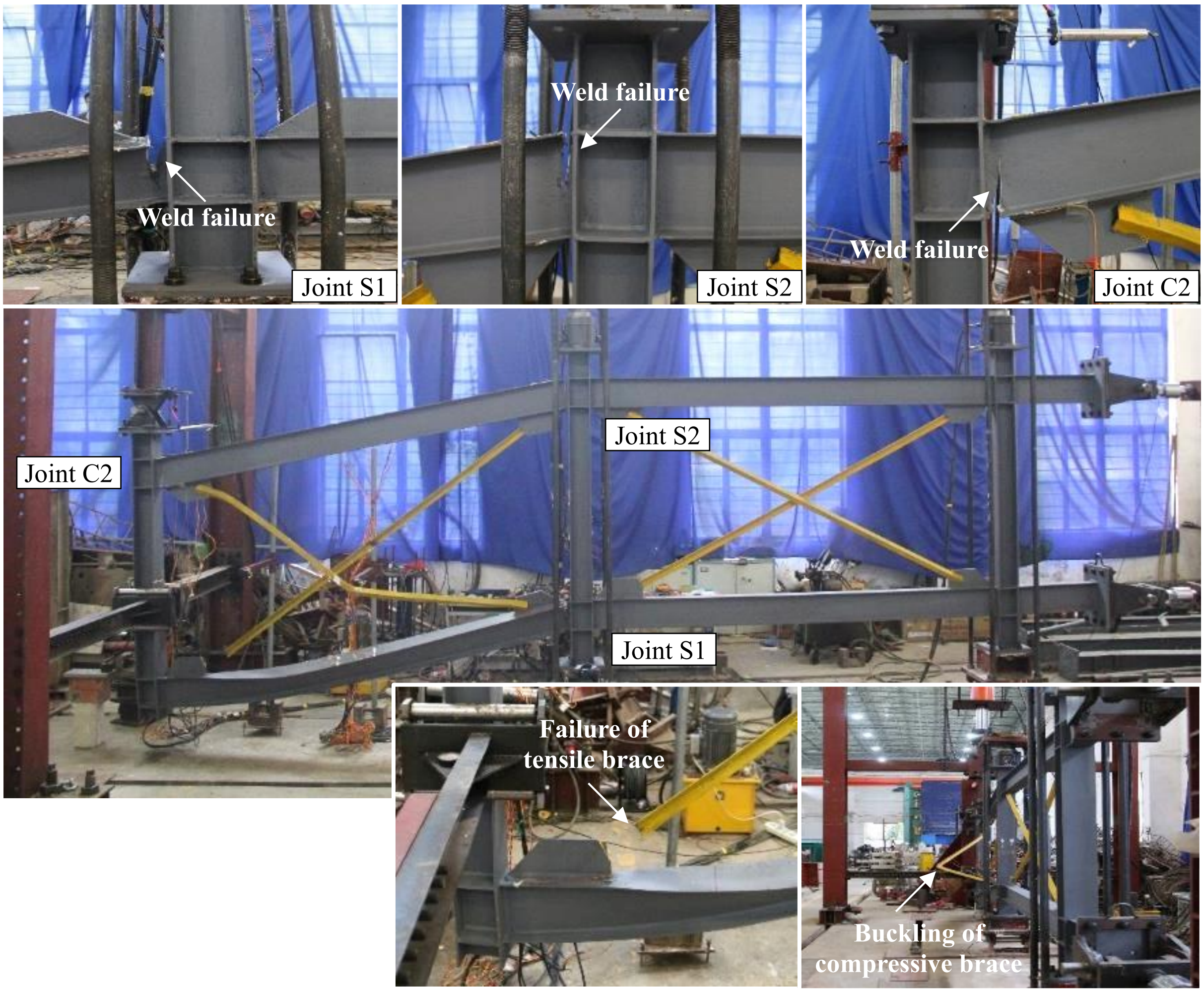

Fig. 7. Failure pattern of Specimen WX

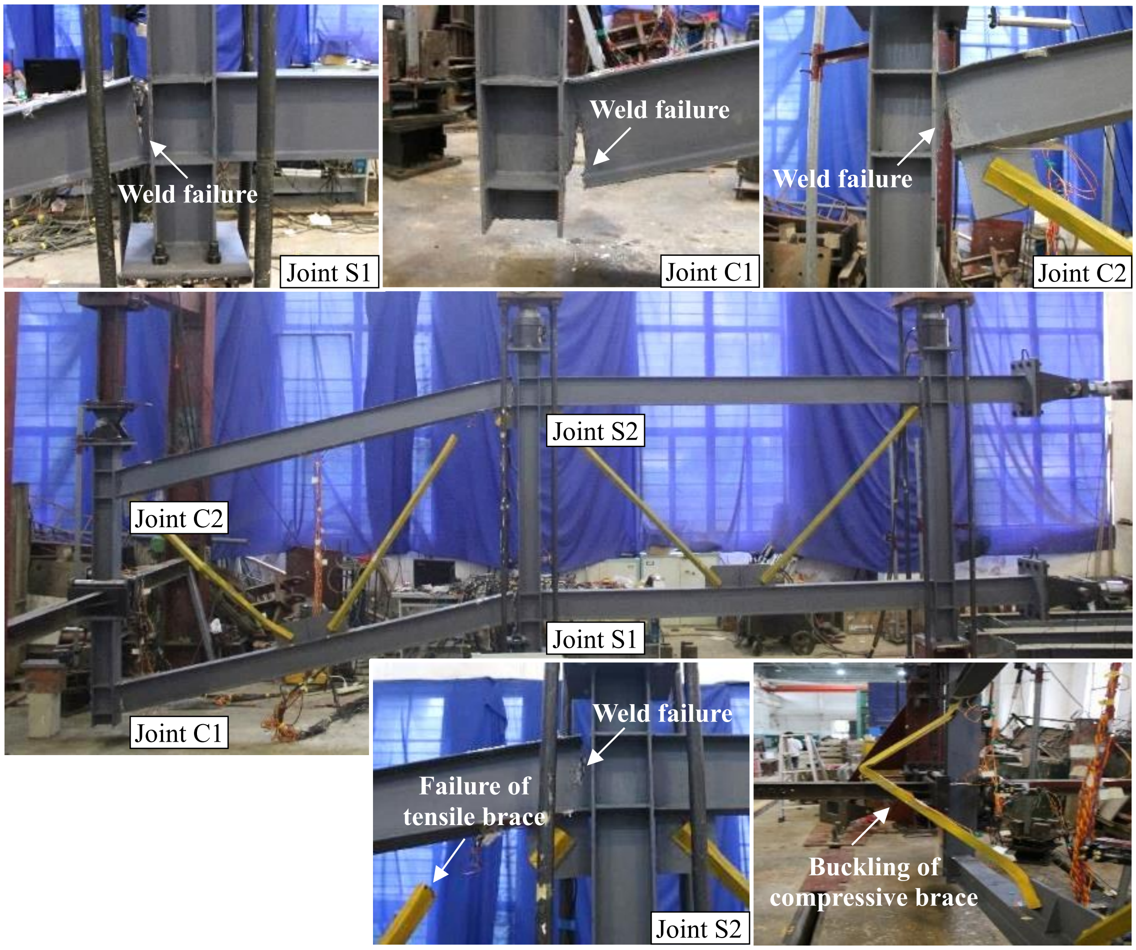

Fig. 8. Failure pattern of Specimen WV

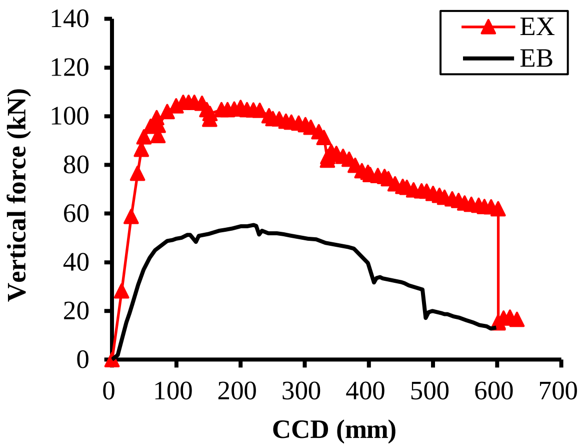

Fig. 9. Load-displacement curves of specimens: EB and EX

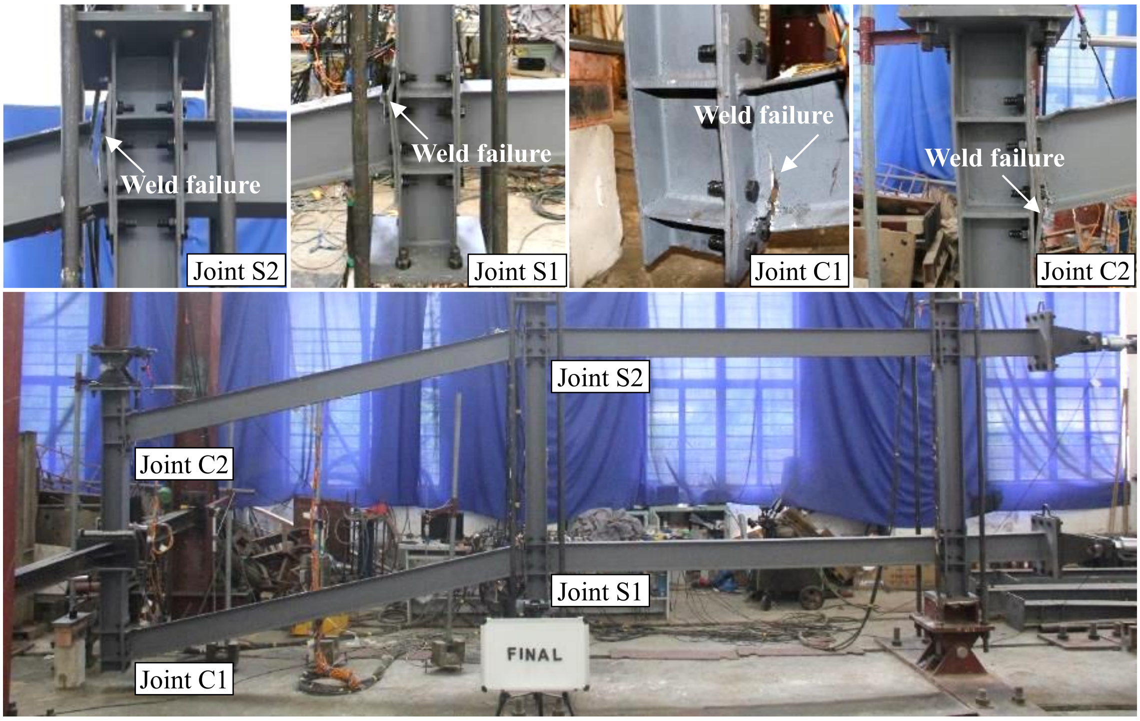

Fig. 10. Failure pattern of Specimen EB

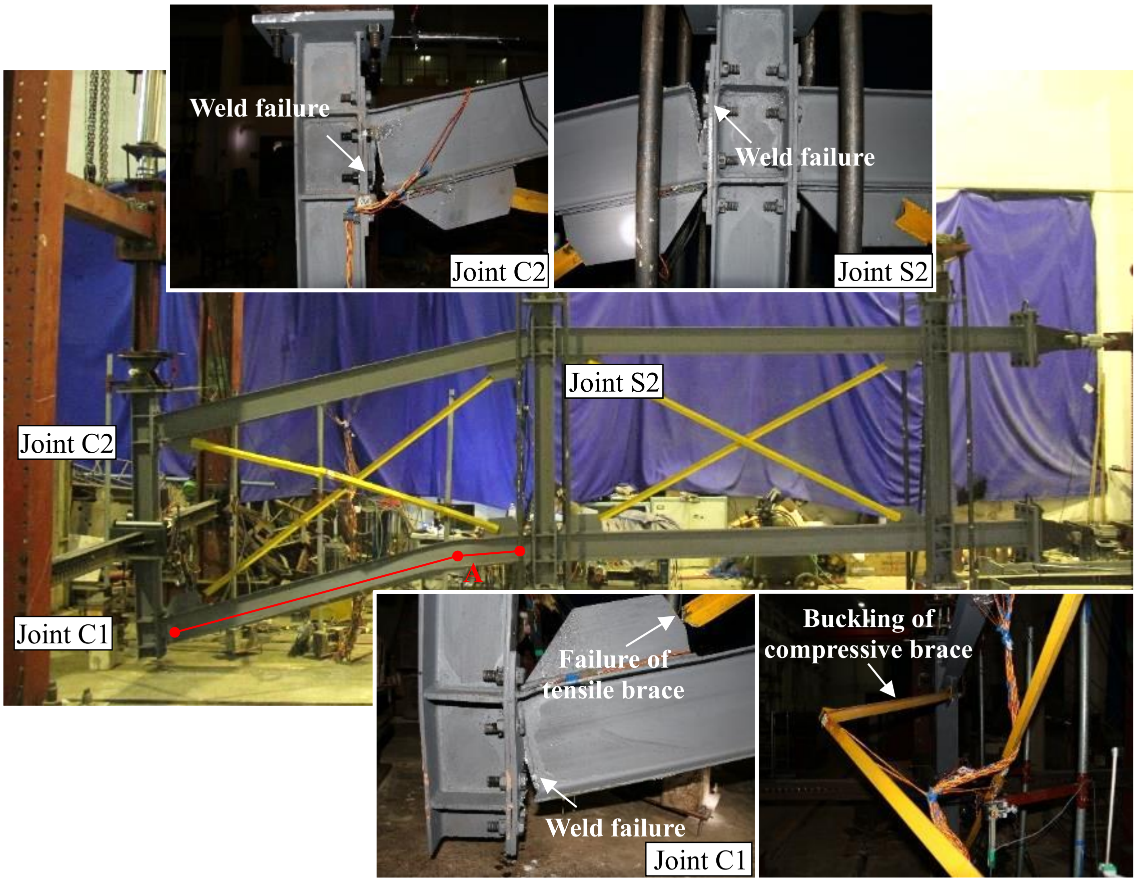

Fig. 11. Failure pattern of Specimen EX

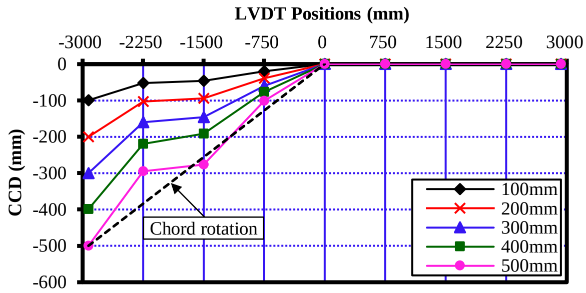

(a)

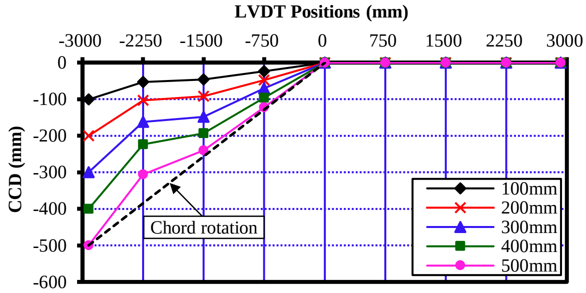

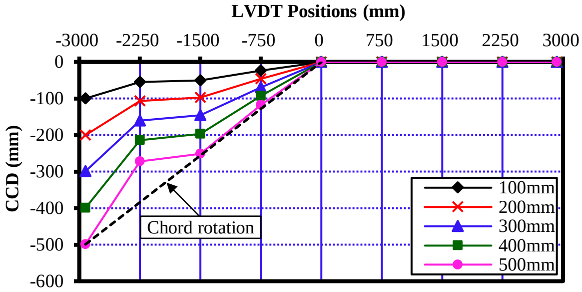

(b) (c)

Fig. 12. Deflection profile of the beams in different stages: (a) WB; (b) WX; (c) WV

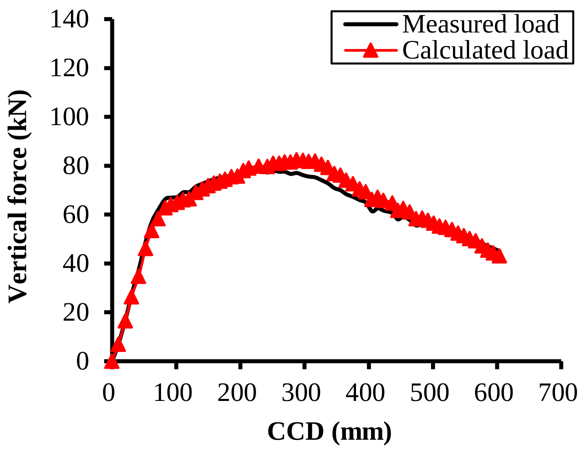

(a)

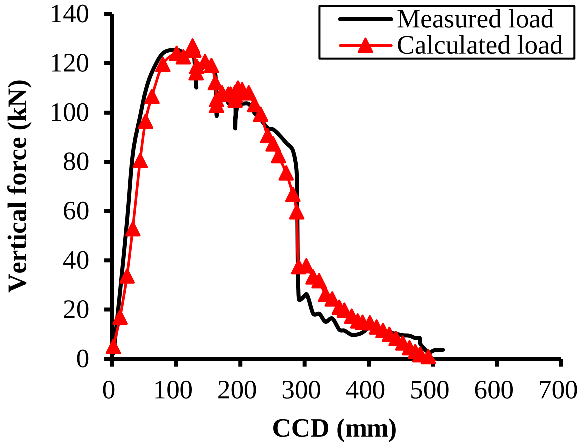

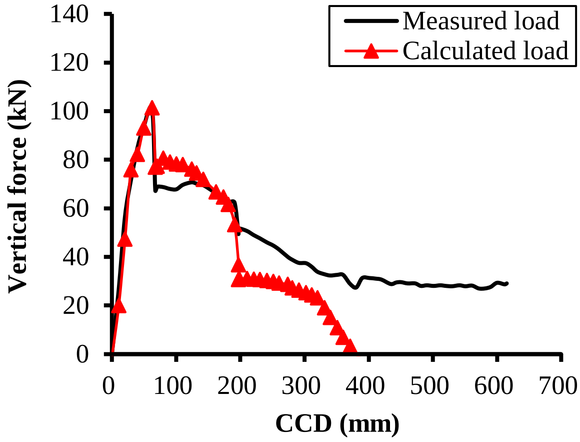

(b) (c)

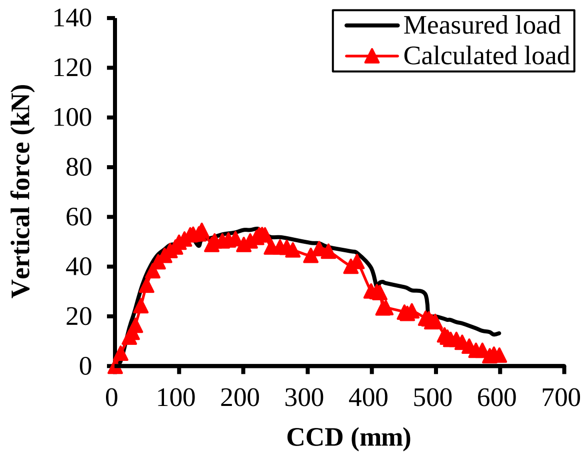

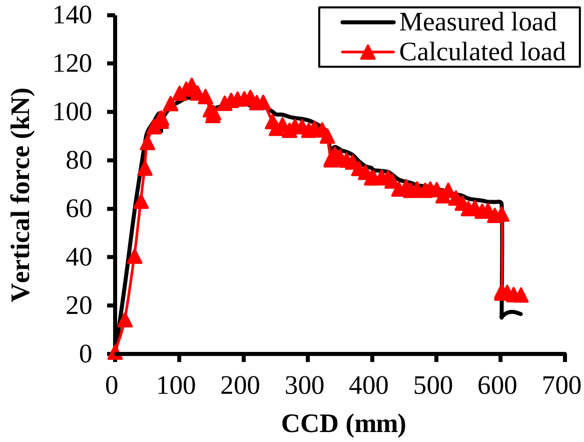

(d) (e)

Fig. 13. Load-displacement curves from strain gauge and load cells: (a) WB; (b) WX; (c) WV; (d) EB; (e) EX

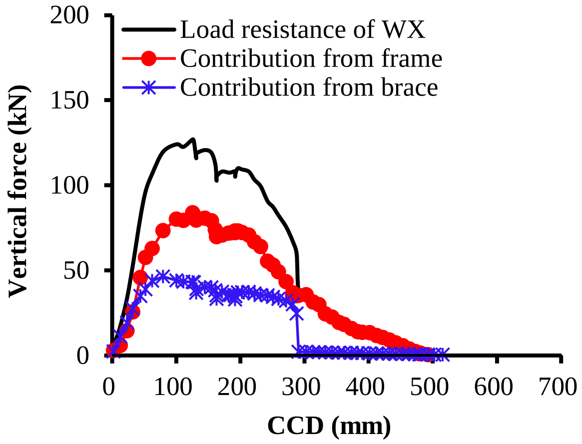

(a)

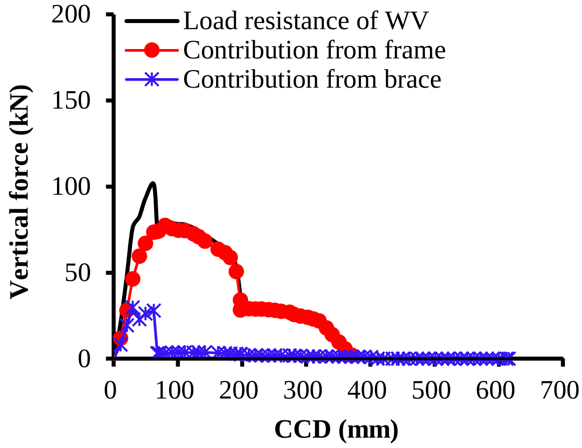

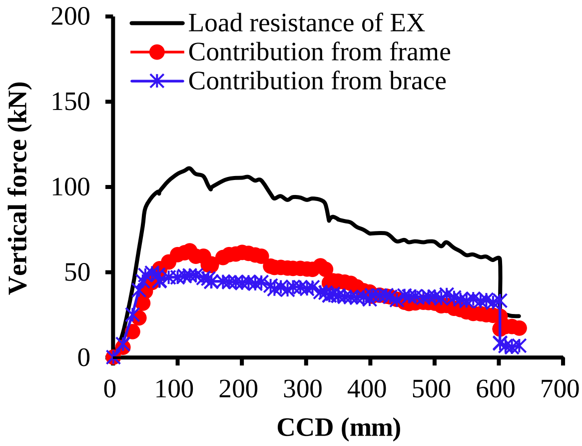

(b) (c)

Fig. 14. De-composition of the load bearing capacity from frame and braces

27

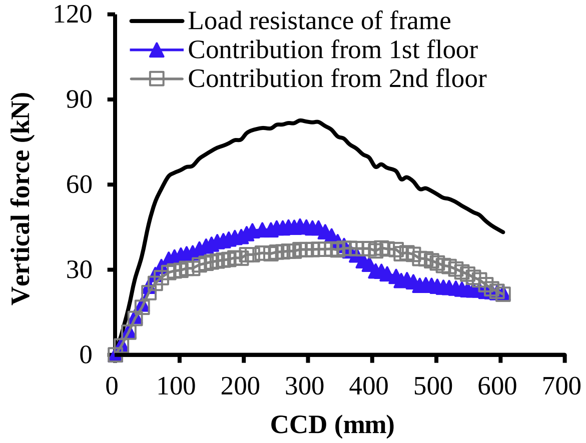

(a)

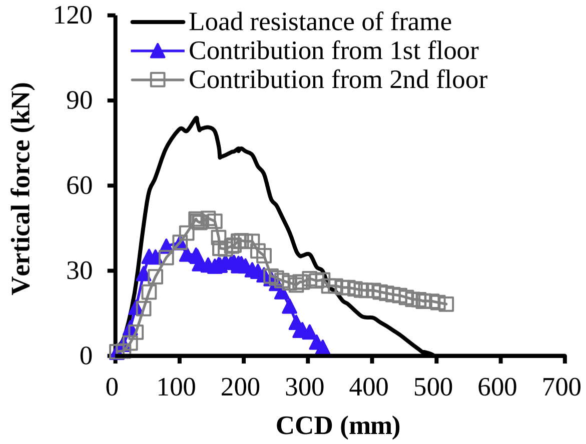

(b)

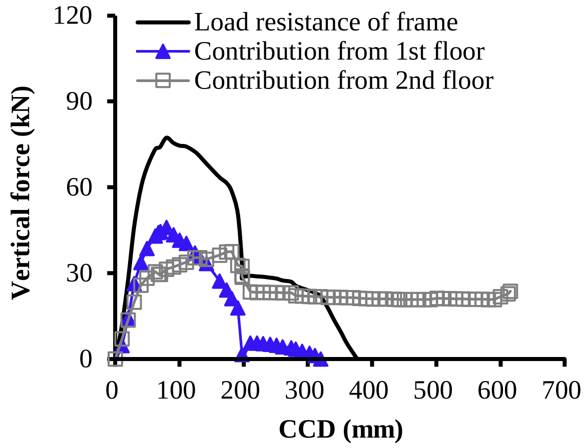

(c)

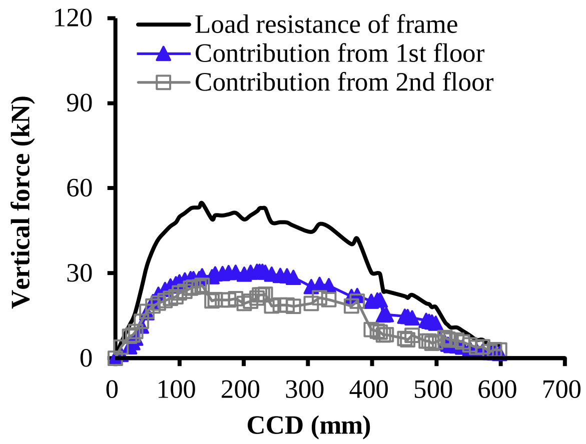

(d)

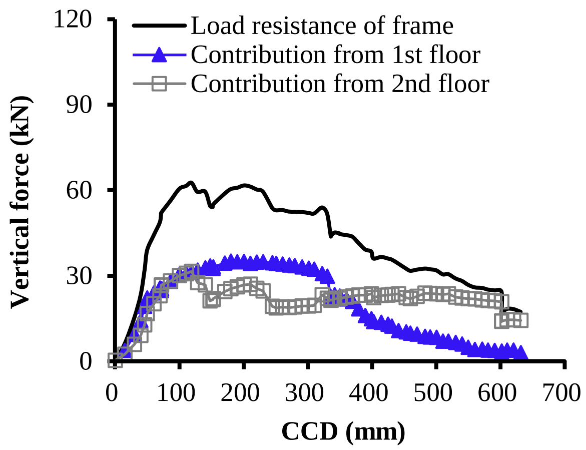

(e)

Fig. 15. De-composition of load bearing capacity from the 1st floor and 2nd floor

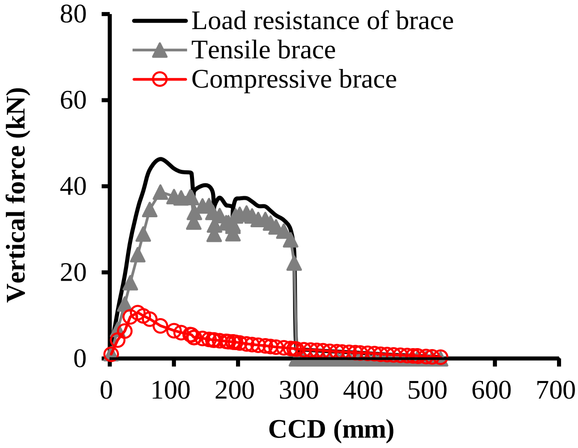

(a)

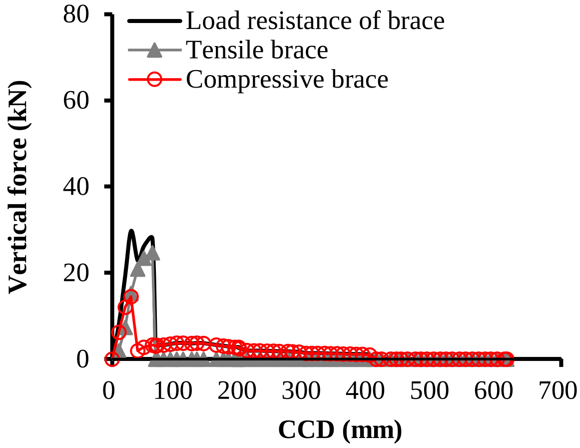

(b)

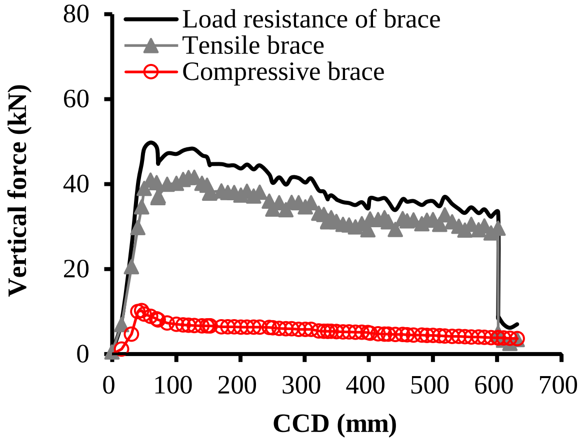

(c)

Fig. 16. De-composition of the load bearing capacity from tensile brace and compressive brace

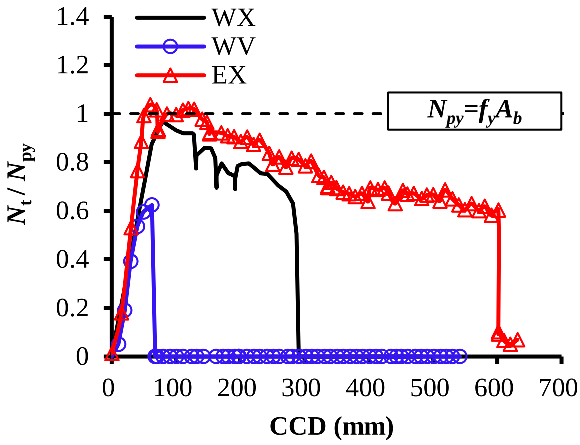

(a)

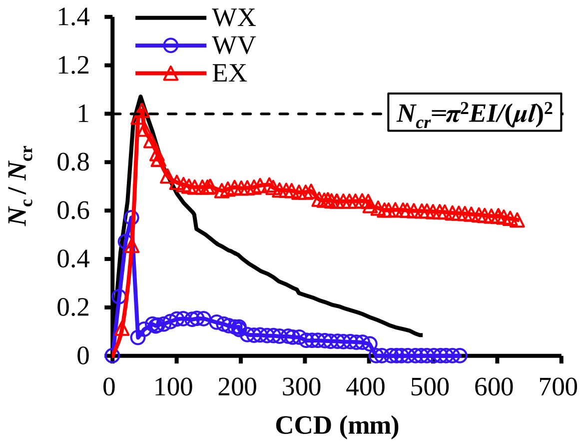

(b)

Fig. 17. Axial force of braces: (a) tensile brace; (b) compressive brace

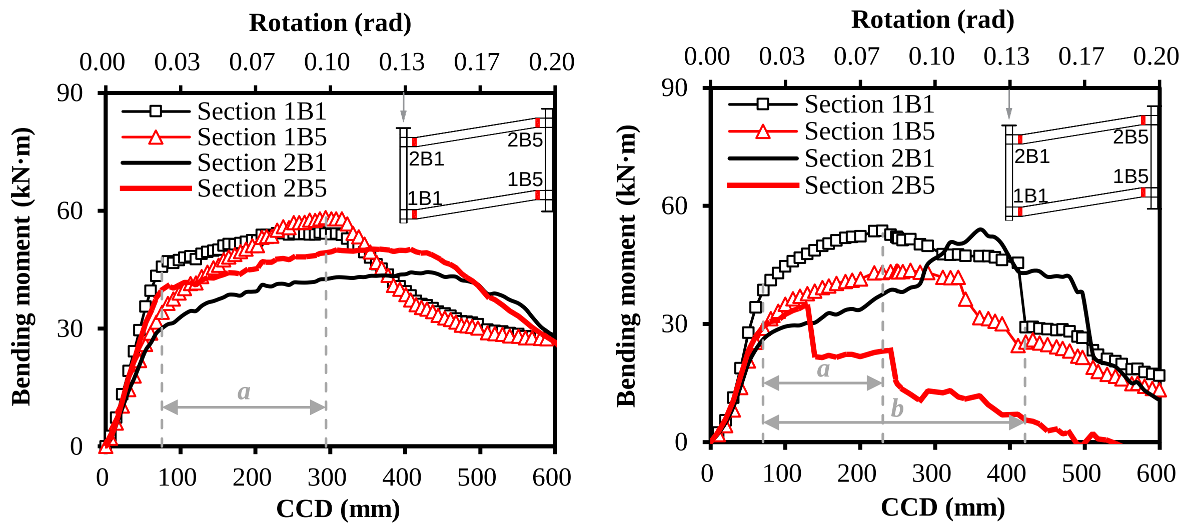

(a) (b)

Fig. 18. Bending moment development at the beam ends: (a) WB; (b) EB

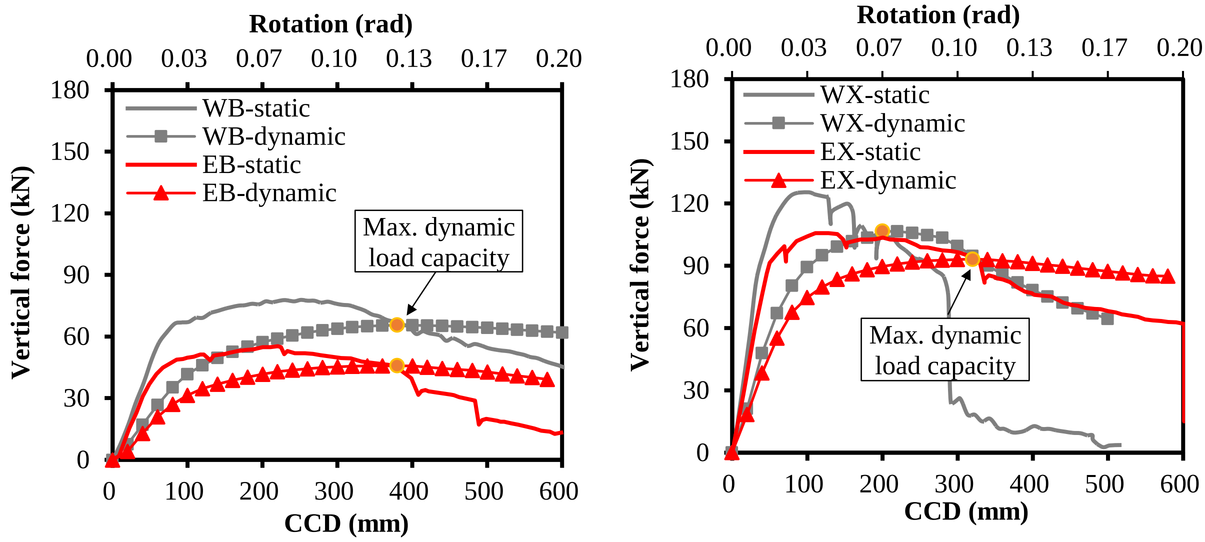

(a) (b)

Fig. 19. Comparison of the static and dynamic load resistance: (a) WB and EB; (b) WX and EX